Table of contents

List of Tables

List of Figures

List of abbreviations

Abbreviation	Meaning
POC	Particulate Organic Carbon
MODIS	Moderate Resolution Imaging Spectrometer
OCM-2	Ocean Color Monitor-2
OLCI	Ocean and Land Color Instrument
SST	Sea Surface Temperature
BoB	Bay of Bengal
Chl-a	Chlorophyll-a
EAV	Emergent Aquatic Vegetation
DOC	Dissolved Organic Carbon
NCF	Nitrate Cellulose Filter
VIIRS-SNPP	The Visible and Infrared Imager/Radiometer Suite-Suomi National Polar-orbiting Partnership
NASA	National Aeronautics and Space Administration
AVHRR	Advanced Very High-Resolution Radiometer
HIRS	High Resolution Infrared Radiation Sounder
TM	Thematic Mapper
CZCS	Coastal Zone Color Scanner
FOV	Field of View
NRL	Naval Research Laboratory
EEZ	Exclusive Economic Zone
NOAA	National Oceanic and Atmospheric Administration
SMI	Standard Mapped Image
APDRC	Asia Asia-Pacific Data Research Center
OB. DAAC	Ocean Biology Distributed Active Archive Center
GPS	Global Positioning System
BNS	Bangladesh Navy Ship
WS	Wind Speed
RMSE	Root Mean Square Error
MRE	Mean Relative Error
SeaWiFS	Sea-Viewing Wide Field of View Sensor

Acknowledgement

At first, all my admiration goes to the supreme creator and Ruler of the universe, the Almighty **Allah** for His great mercy to keep me alive and enables me to pursue my education in Fisheries and Marine Resource Technology Discipline as well as to complete my work for the degree of Master of Science in Coastal and marine Science.

I would like to express my sincere gratitude and profound appreciation to my honorable supervisor, **Mohammad Abdur Rouf**, Professor and Head, Fisheries and Marine Resource Technology Discipline, for his continuous guidance, valuable suggestions, critical observations and sustained support in writing this thesis.

I recall with warm appreciation and great indebtedness or the support, guidance and suggestions extended to me by all my respected teachers in Fisheries and Marine Resource Technology Discipline, Khulna University.

I would also like to give special thanks to **Bangladesh Navy** for collecting water samples from the Bay of Bengal with the ship **BNS Turag.** I am thankful to Mr. Aminul Islam, a geo-specialist consultant of WorldBank, for his continuous support to work in ArcGIS tools.

Special thanks go friends **Zareen Afroje** for his support for completing my thesis work in laboratory. I would thank to thank **Mr. Hriday Molla**, a graduate student of Urban and rural Planning Discilpine for his support. I specially thank to my senior Al-Hasan Antu, a post-graduate student of Khulna university for giving me necessary direction to complete my thesis.

I would like to acknowledge Khulna University Research Cell (KURC) for their essential supports.

Finally, I would like to express my very profound gratitude to my parents for all care, unfailing support and continuous encouragement throughout my study. This accomplishment would not have been possible without them.

Md Rony Golder
Student ID: MS 190660
Coastal and Marine Science,
FMRT Discipline
Khulna University,
June 2020

Abstract

Particulate Organic Carbon (POC) plays a vital role in ocean carbon cycle and is linked to many important ocean biogeochemical processes. This study aims to investigate the seasonal variability of POC and its association with Sea Surface Temperature (SST), Chlorophyll-a (Chl-a) and wind vector in the Bay of Bengal (BoB) of Bangladesh part, as well as to validate satellite data with in-situ measurement data. Moderate Resolution Imaging Spectroradiometer (MODIS) Aqua satellite level-3 data of POC, Chl-a and SST were used in this study. Wind vector data were obtained from WindSat Polarimetric Radiometer satellite. Monthly averaged POC (2002-2019) was ranged from 103.08 to 184.22 mgm^{-3} with an average of 154.28±31.47 mgm^{-3}. The POC was higher (181.80 ±22.34 mgm^{-3}) during the northeast-monsoon (December-February), and lower (136.56±36.24 mgm^{-3}) in the pre-monsoon (March-May). Statistically significant ($F_{(3,202)}$ =18.09; p<0.05) difference of POC was found among the seasons. A very weak inverse relationship was found between POC and SST whereas POC and Chl-a showed a positive relation for all the seasons in the BoB. This study revealed that the POC was very prominent with the wind vectors prevailing northeasterly in northeast and post monsoon and low with the southwesterly wind in southwest and pre monsoon. POC variability was mostly influenced by Chl-a than SST and wind vector for BoB. Variability of POC in BoB is mainly influenced by monsoon effect which causes tremendous rainfall and strong wind. A significant (p<0.05) moderate correlation (r=0.74) was found between the MODIS Aqua satellite data and in-situ observation. Further detailed investigation is required to observe the association of other parameters with POC variability.

1. Introduction:

Particulate organic carbon (POC) is one of the most important pools of organic carbon found in the ocean. It takes part in various biological process and influences both organic and inorganic carbon cycles (Liu et al., 2019b) and composed of living materials (Phytoplankton, zooplankton, bacteria, etc.) and detritus. Particulate organic carbon is an important pathway by which organic carbon (formed via photosynthesis) is transferred from the surface to deeper ocean layers where it may be sequestered. It is often used as an indicator of productivity in the euphotic zone (Fingas, 2018). Some zooplankton, such as appendicularians and pteropods, discard gelatinous materials in the surface waters as part of their normal activities. These materials can account for extremely high local POC values in the surface waters (Wangersky, 1977). Although particulate organic carbon (POC) is only 1–10% of dissolved organic carbon (Parsons 1975) in the seawater, the study on POC has become a hot topic of marine sciences because of its importance in marine food chain and marine productivity (Shen, Zhiliang; Yang, Heming & Liu, 2020).

One of the main sources of POC input to estuaries is by their associated rivers (Bianchi and Bauer, 2012). On a global scale, rivers deliver approximately 2.0×10^{8} t C/yr. of POC into marginal seas (Liu et al., 2019a). The photosynthetic fixation of inorganic carbon and nutrients into plant biomass is the ultimate source of POC in estuarine and coastal systems. The consumption and transformation of organic matter through metazoan and microbial (e.g., microbial loop) trophic levels are critical in the cycling of POC in estuaries and coastal systems (Bianchi et al., 2007; Wetzel, 1995).

POC concentration in ocean is affected by phytoplankton (Fernandes et al., 2009) in association with physical parameters like; light, nutrients, chlorophyll-a concentration, salinity, temperature (Stramska, 2014). Except this, terrigenous POC transported by river discharge (Wang et al., 2012). riverbed erosion (Xu and Milliman, 2009), current (Fan et al., 2018), wind speed and tidal flow (Liu et al., 2019b), SST (Fernandes et al., 2009) also responsible for POC contribution in ocean. Seasonal and annual variations in hydrology, including storm and hurricane events, further influence the input, dispersion, and cycling of POC. Several studies have indicated that remineralization and remobilization also play important roles in controlling POC variation on the shelf (Le et al., 2017).

The global ocean surface wind vector (wind speed and direction) field provides essential environmental information. It is critical data for short-term weather forecasts and warnings,

nowcasting, climatology, and oceanography studies (Gaiser et al., 2004). Wind can enhance sediment resuspension and vertical mixing (He et al., 2013). So, wind vector is an important factor for the variability of POC concentration in the ocean.

POC is composed of suspended particles whose light absorption and back scattering features can be recorded by satellite sensors. (Liu et al., 2019b). The use of satellite-based sensors to estimate POC in the estuary, lakes and global ocean provides numerous advantages with respect to standard field measurement (Le et al., 2017; Liu et al., 2015; Stramski et al., 1999a). The efficiency of satellite measurement depends on the optical characteristics of the water body. There are several satellite systems in operation today that collect imagery that is subsequently distribute POC data to users such as MODIS Aqua (Moderate Resolution Imaging Spectroradiometer), Oceansat-2 (OCM-2: Ocean Color Monitor-2) and other satellites which have Chl-a absorption bands like Sentinal-3 (OLCI- Ocean and Land Color Instrument), Landsat 8. Among these, MODIS (or Moderate Resolution Imaging Spectroradiometer) Aqua data is frequently used to estimate the distribution of POC in different parts of world ocean (Duan et al., 2014).

Recently, spatial and temporal variability of POC have been studied in Yellow Bohai sea Surface POC is highest in spring (452 ± 53.6 mgm^{-3}) in the Yellow Bohai Sea in China, and lowest in summer (245 ± 84.8 mgm^{-3}) in this sea (Fan et al., 2018). The spatial and seasonal patterns of POC are due to combined influences of primary productivity, water exchange, sediment resuspension and terrestrial inputs. Le et al., (2019) studied POC of two riverbed estuaries in the north Gulf of Mexico. They found that POC concentration may change with changing of season. POC in winter and spring was higher than summer and fall. It also changes with year basis. The highest measured POC occurred in March 2003, with a mean value of 506.1±442.2 mgm^{-3} and a median value of 353.0 mgm^{-3}. The lowest POC occurred in November 2003, with a mean value of 310.6±324.0 mgm^{-3}. Liu et al., (2015) studied POC distribution in pearl river estuary, China. They found that in situ POC concentrations were ranged between 0.4 mgm^{-3} and 0.6 mgm^{-3}. The monthly decrease trend of POC concentration was mainly driven by its significant decrease in wet season (May to October) due to low flow velocity, sediment resuspension (Liu et al., 2019a).

Many researches work have been done for understanding the variability of POC distribution in different ocean such as Pacific (Fan et al., 2018; Pavia et al., 2019), Atlantic (Stramska, 2014), Southern ocean (Zhu et al., 2011) and global scale (Gardner et al., 2006; Stramska, 2009;

Świrgoń and Stramska, 2015). However, little information is available on the distribution of POC in the Indian Ocean (Bhosle et al., 1988) in general, and in the Bay of Bengal (Fernandes et al., 2009; Nandakumar et al., 1987) in particular where the large-scale and long time series data and analysis are insufficient. Remarkably, no study has been conducted yet emphasizing the seasonal variability of POC in the Bangladesh part of BoB. In addition, there is a lack of research on the relationship between changes in POC and other parameters (physical and environmental) in this sea.

Satellite data indicate a decrease in the global primary productivity meaning that there is a negative trend in POC in global ocean. The decrease of POC concertation per year could indicate that the biological carbon cycle in the ocean is weakening (Xie et al., 2019). Hence, a baseline study is required to know the level and distribution of POC and associated influencing factors and their level of contribution on the variability which would give us the health status of the marine ecosystems by providing a means for advancing a methodology to diagnose rates and fluxes of relevance to the global carbon cycle and to constrain the uncertainties of carbon budgets. This gap is the motivation of this research to understand more about the seasonal distribution of POC in the BoB and the relationship between POC and other parameters.

In the present research, we considered 18 years (2002-2019) POC data value for estimating seasonal variability of POC in the BoB following the data collected from MODIS Aqua satellite.

Objectives of the Research

- To identify the seasonal trends of POC distribution.
- Find out season wise relationship between POC and SST in the BoB.
- Find out season wise relationship between POC and Chl-a in the BoB.
- Find out season wise relationship between POC and wind vector.
- To validate the MODIS Aqua satellite based POC with and in situ measurements.

2. Review of Literature

2.1 Particulate organic carbon (POC)

Marine organic carbon exists in 3 forms, which are dissolved, particulate and volatile. Although particulate organic carbon (POC) in the seawater is only 1–10% of dissolved organic carbon , because of its importance in marine food chain and marine productivity, the study on POC has become a hot topic of marine sciences (Shen, Zhiliang; Yang, Heming & Liu, 2020). Particulate organic carbon in seawater includes two (life and non-life) components. Life component includes microbial bacteria, fungi, phage, microorganism photosynthetic plankton, zooplankton, small fish and shrimps and large marine mammals. Non-life part is also known as organic debris, including marine biological activity generated during the wreckage and debris(Zhu et al., 2011). Particulate organic carbon (POC) is an important form of oceanic carbon form, taking part in various biogeochemical processes and influencing both organic and inorganic carbon cycles (Bai et al., 2015; Liu et al., 2019b; Stramski et al., 1999b)

2.2 Abundance of POC in ocean

One of the main sources of POC input to estuaries is by their associated rivers. Inputs from rivers will depend on a variety of factors involving both the river itself and the specific estuary (Bianchi and Bauer, 2012). On a global scale, rivers transport about 200 Tg C (Tg=1×10^{12} g) of terrigenous POC to marginal oceans annually (Wang et al., 2012). The distribution of dissolved, total particulate, and living particulate organic carbon in the surface (0-300 m) and deep ocean (>300m) are varied and summarized in Table 1 (Murray, 2000).

Table 1 Abundance of POC according to the depth

Depth (m)	Dissolved (10^6 tonnes C)	Approximate concentration (µgC/L)	Particulate (10^6 tonnes C)	Approximate concentration (µgC/L)
0-300[a]	110000	1000-1500	11000	100
300-3800[b]	630000	500-800	13000	3-10
	740000 [c]		24000[c]	
Total	670000[d]		14000[d]	
	1000000[e]		30000[e]	

[a]Concentrations vary widely with geographical area and with season. The depth at which the concentration tends to approach a constant level varies widely from 100 to 500 m.
[b]Concentrations more constant.
[c](Williams, 1971)
[d](Menzel, 1974)
[e](Williams, 1975)

2.3 Sources of POC

The photosynthetic fixation of inorganic carbon and nutrients into plant biomass is the ultimate source of POC to estuarine and coastal systems. However, these sources may be derived from a vast range of primary producers in aquatic and terrestrial environments (Bianchi, 2007). In addition to autochthonous estuarine sources, inputs of POC to estuaries can occur from a variety of marine, riverine, and terrigenous end members, which may support both estuarine autotrophic and heterotrophic production (Fig. 1).

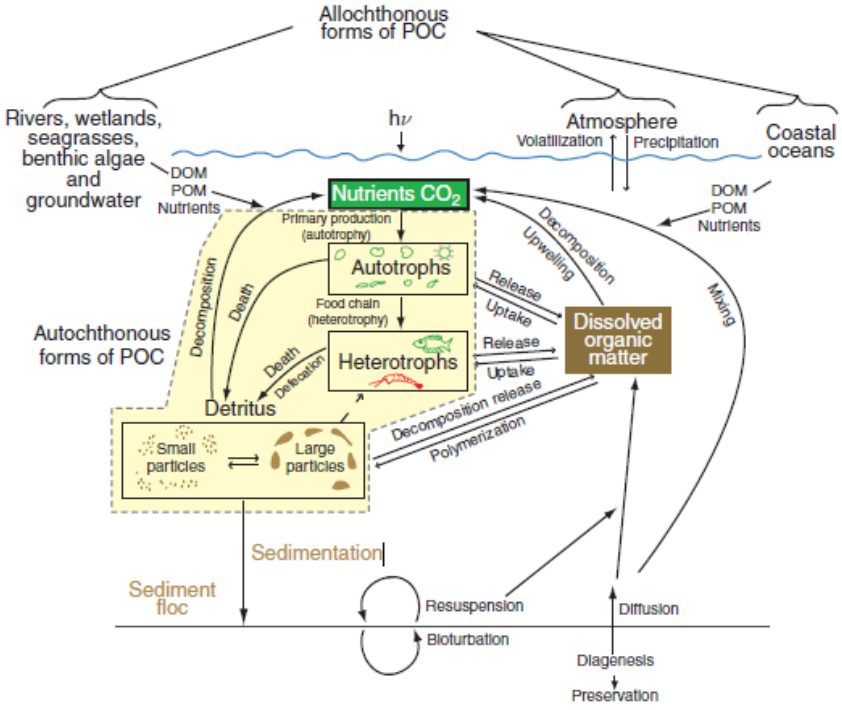

Fig. 1 Biogeochemical cycling of nutrients, DOM, and POM, in the estuary proper bound by coastal ocean and riverine end-member exchange (Bianchi and Bauer, 2012)

2.3.1 Terrestrially Derived POC

The tectonically driven uplift of marine sedimentary rocks above sea level on the Earth's surface over geological time produces rock material that can be altered into soils and sediments by weathering processes. Chemical weathering processes in soils are important in the transformation of primary to secondary minerals. Particularly important for the formation of suspended POC in rivers and estuaries is the weathering of feldspars (the most abundant group of minerals in the Earth's crust), K-feldspar is transformed to kaolinite (a clay) through the following reaction:

$KAlSi_3O_8 + H_2CO_3 + H_2O \rightarrow Al_2SiO_5(OH)_4 + 2K^+ + 4H_4SiO_4 + HCO_3^-$ (K-feldspar) (kaolinite)

During the formation of kaolinite, dissolved K^+ ion is released from soils, while Al is retained in the solid-phase clay mineral product. Particle–particle and particle–dissolved constituent interactions in river and estuarine systems, have broad-reaching effects on biogeochemical cycling of carbon and other biogenic elements in both dissolved and particulate phases in estuaries because of the strong linkages between the transformation and composition of clay minerals in drainage basin soils and estuarine sediments (Bianchi, 2007).

2.3.2 Estuarine Algal Production

Phytoplankton and other primary producers (Fig. 1) represent a quantitatively significant source of POC to most estuaries. Seasonal changes in estuarine phytoplankton abundance and composition are controlled by changes in riverine inputs, nutrients, tidal variability, algal respiration, light availability, horizontal exchanges, and consumption by grazers (Battin et al., 2008; Boyer et al., 1993; Boynton et al., 1982; Cloern, 1996; Lucas and Cloern, 2002; Malone et al., 1988; O'Donohue and Dennison, 1997; Thompson, 1998). Benthic macroalgae and microphytobenthos are also important sources of POC in estuaries (De Jonge and Colijn, 1994; Gould and Gallagher, 1990; Pinckney and Zingmark, 1993; Rizzo et al., 1992; Sullivan and Moncreiff, 1990). However, there is increasing evidence that macroalgae and microphytobenthos may be at least as important as phytoplankton in shallow environments in terms of total biomass and POC production (Cahoon, 2002; Dalsgaard, 2003; Webster et al., 2002).

2.3.3 Submerged and Emerged Aquatic Vegetation

Seagrass meadows may also be prominent producers of POC in many shallow littoral habitats in estuarine systems of the South Atlantic Bight (Den Hartog, 1970; Green et al., 2003; Hemminga and Duarte, 2000).The submerged canopy of estuarine seagrass systems has been found to decrease shallow-wave energy, thereby allowing for more efficient trapping of suspended particles and POC derived from both autochthonous and allochthonous sources (Fonseca and Kenworthy, 1987; Ward et al., 1984). Tidal freshwater marshes and mesohaline salt marshes, and mangrove systems have been found to be major sources of primary production and EAV POC in estuarine systems (Fonseca and Kenworthy, 1987; Ward et al., 1984).

The global export of POC from mangroves and salt marshes varies significantly between specific systems, but generally ranges between approximately 2–420 and 27–1052 gCM−2 yr−1, respectively (Alongi et al., 1989).

2.4 Environmental factors associated with POC

2.4.1 Chlorophyll

Chlorophylls are ubiquitous pigments in the plant kingdom that play a key role in photosynthesis, a vital function for life on Earth (Roca et al., 2016). There are different classes of chlorophylls, major of them are chlorophyll-a (Chl-a) and chlorophyll-b (Chl_b). Chlorophyll-a (Chl-a) is a primary form of chlorophyll used in photosynthesis. It absorbs light energy from wavelengths of violet-blue and orange-red light, and it reflects green/yellow light, thus resulting in the observed green color of most plants. Because it is essential for photosynthesis in plants as well as plankton in the sea, detection of chlorophyll has become a well-established method used by various satellite systems (Fingas, 2018). The phytoplankton abundance played an important role in controlling the concentrations of POC. This was evident from the fairly good significant positive correlations of the concentrations of Chl-a with the concentrations of POC (Fernandes et al., 2009; Zhu et al., 2011).

2.4.2 Sea surface temperature (SST)

Sea surface temperature (SST) is a strong indicator of productivity, pollution, and global climate change. It has been used to identify sources of pollution, thermal pollution, upwellings, and areas of variant productivity. It is also an indicator of stress to corals and other species (Fingas, 2018). On the landward side of the front, there was a sharp decline in SST as well as an abundance of phytoplankton biomass. On the seaward side of the front, they observed an increase in SST as well as a decrease in the amount of phytoplankton biomass (Kavak and Karadogan, 2011). As chl shows positive relation with POC concentration, POC shows inverse relation with SST.

2.4.3 Wind speed

The global ocean surface wind vector (wind speed and direction) field provides essential environmental information. It is critical data for short-term weather forecasts and warnings, nowcasting, climatology, and oceanography studies(Gaiser et al., 2004). Wind can enhance sediment resuspension and vertical mixing (He et al., 2013). In winter, strong wind strengthens tidal currents, leading to intensive sediment resuspension. POC concentrations were positively correlated with wind speed (Liu et al., 2019a). Water circulation on the inner shelf is primarily

driven by wind. Easterly winds prevail during autumn, winter and spring, which drives westerly surface currents along the shelf, and thus, river plume is confined along shelf regions west of the outflows. In the summer, southerly winds reverse the local circulation and promotes an eastward transport of the river plume. A similar effect of wind and surface currents on POC patterns was also found to vary by season (Le et al., 2017).

2.4.4 Water and sediment fluxes

Large riverine water flow strengthens water stratification and weakens vertical mixing (Shen et al., 2013). As a result, POC concentration becomes low in the wet season of the outer BoB. On the other hand, basin and riverbed erosion add POC (Xu and Milliman, 2009).

2.4.5 Tidal processes

With high water velocity, bottom sediment was resuspended and dispersed to the water surface. As a result, surface POC concentrations were high with high water velocity. Surface POC concentration decreased during the late period of tidal ebbing and early period of tidal flooding with low water velocity; the same pattern was observed during the late period of tidal flooding and early period of tidal ebbing (Liu et al., 2019a).

Table 2 Other factors associated with POC

Name of Factors	Relationship with POC	References
Phytoplankton	Positive	(Stramska, 2014)
Light	Positive	(Fernandes et al., 2009)
Nutrients	Positive	(Fan et al., 2018)
Upwelling	Positive	(Stramska, 2014)
Riverine Water flow	Negative	(Shen et al., 2013)
Riverbed erosion	Positive	(Xu and Milliman, 2009)
Current	Positive	(Fan et al., 2018)
El nino	Negative	(Stramska, 2009)

2.5 Trends of POC

The spatial and temporal variations of POC in the Yellow-Bohai Sea over 2002–2016 were studied (Fan et al., 2018). A research has been done on satellite observations of seasonal and regional variability of POC concentration in the Barents Sea (Stramska and Bialogrodzka,

2016). Comparison of in situ and satellite ocean color determinations of POC concentration in the global ocean have been done (Świrgoń and Stramska, 2015). Another research for observing POC in global ocean have also been done from SeaWiFS ocean color (Stramska 2009).

Seasonal and inter annual variability of particulate organic carbon within the Southern Ocean from satellite ocean color observations have been studied (Allison et al., 2010). Distribution and source analyses of POC in the Yellow and Bohai Sea during summer, 2013 have also been observed (Haibo et al., 2016). A study has been done on spatial and temporal variations of POC sinking flux in global ocean from 2003 to 2018 (Xie et al., 2019). A study has been done for validation and inter comparison of ocean color algorithms for estimating POC in the oceans (Evers-King et al., 2017). A research have been done for finding distribution and sources of POC in the Yellow Sea and East China Sea (Cheng et al., 2011). A different kind of research on POC have been done for investigating remotely sensed detection and application analysis of ocean POC (Cong et al., 2012). Research based on POC have also been done in river and estuary. For example researches have been done for satellite observation of POC dynamics in two river-dominated estuaries (Le et al., 2017) and RS observation of POC in the Pearl River Estuary (Liu et al., 2015) and temporal variability in terrestrially-derived sources of POC in the lower Mississippi River and its upper tributaries have also been studied (Bianchi et al., 2007).

Spatial and temporal distribution of particulate organic carbon in Yellow Sea and East China Sea have been studied (Shi et al., 2011). Variability of particulate organic carbon in inland waters have been observed from MODIS Aqua imagery (Duan et al., 2014). A color-index based empirical algorithm for determining POC concentration have been done in the ocean from satellite observations (Le et al., 2018). Satellite-derived POC flux in the Changjiang River through different stages of the Three Gorges Dam have been observed (Liu et al., 2019a). POC and Its composition in Jiaozhou Bay have been obsereved in 2019 (Shen, Zhiliang; Yang, Heming & Liu, 2020). Seasonal and spatial distribution of particulate organic matter in the Bay of Bengal was observed (Fernandes et al., 2009)

Few studies related to POC have been found in recent years in BoB but most of the studies focused on the southern (Indian) part of BoB. Therefore, there is a sever scarcity of POC information in the Northen (Bangladesh) part of BoB using satellite data.

2.6 Effect on Marine Life

Ocean carbon cycle: Particulate organic carbon (POC) is an important form of oceanic carbon form, taking part in various biogeochemical processes and influencing both organic and inorganic carbon cycles It can sequester carbon, scavenge associated elements and compounds, and sink to the deep ocean as part of the "biological pump". Land and ocean ecosystems, which are the two largest active carbon reservoirs in the world, are connected by rivers (Bai et al., 2014; Wang et al., 2012).

POC in the ocean is also added through local phytoplankton production, flocculation of dissolved organic carbon (DOC), and sediment resuspension, etc. Oceanic POC can also be removed through trans formation of POC to DOC, microbial respiration, and particle deposition, etc. Due to these physical and biogeochemical properties, investigating the variations in marine POC using in-situ data from ships or other platforms remains challenging (Liu et al., 2019a).

Under the influence of the East Asian monsoon, Asian river watersheds are characterized by high POC yields (Ludwig et al., 1996). POC concentration in summer is usually higher than that in winter.

2.7 Estimation of POC

POC is measured from both in situ (ship base) and satellite data. In ship base-based management, There are many analytical methods for the measurement of POC distribution (Biddanda and Benner, 1997; Knap et al., 1996; Parsons et al., 1984; Sharp, 1974). Among the most used method for the POC estimation is the spectrophotometric method and this is done for the validation of remote sensing data (Parsons et al., 1984). Water samples will be collected from different location of Bay of Bengal with the help of Bangladesh Navy. Then it will be immediately filtered through pre-combusted (100^0C 1h) 47mm NCF/C (0.45µm pore size) nitrocellulose filter. Filters will be stored at -20^0C until the analysis will be completed. Particulate matter left on the filters will be analyzed for POC. As the filters will not be pre-weighed, suspended matter could not be determined on these samples. POC will be analyzed spectrophotometrically after wet oxidation of carbon by acid dichromate (Parsons et al., 1984).

POC is composed to suspended particles whose light absorption and back scattering features can be recorded by satellite sensors. (Liu et al., 2019b). The use of satellite-based sensors to estimate POC in the estuary, lakes and global ocean provides numerous advantages with respect to standard field measurement(Le et al., 2017; Liu et al., 2015; Stramski et al., 1999a).

The efficiency of satellite measurement depends on the optical characteristics of the water body. There are several satellite systems in operation today that collect imagery that is subsequently distribute POC data to users such as MODIS Aqua (Moderate Resolution Imaging Spectroradiometer) (Duan et al., 2014), SeaWiFS (Stramska, 2009), The Visible and Infrared Imager/Radiometer Suite including the Suomi National Polar-orbiting Partnership (VIIRS-SNPP) (Lee et al., 2019). MODIS (or Moderate Resolution Imaging Spectroradiometer) Aqua data is frequently used to estimate the distribution of POC in different parts of world ocean (Evers-King et al., 2017; Gardner et al., 2006; Le et al., 2018; Liu et al., 2019a, 2019b; Zibordi and Mélin, 2017).

2.8 MODIS Aqua Satellite

The Moderate Resolution Imaging Spectroradiometer (MODIS), is a 36-band spectroradiometer measuring visible and infrared radiation and obtaining data that are being used to derive products ranging from vegetation, land surface cover, and ocean chlorophyll fluorescence to cloud and aerosol properties, fire occurrence, snow cover on the land, and sea ice cover on the oceans. The first MODIS instrument was launched on board the Terra satellite in December 1999, and the second was launched on Aqua in May 2002.

Instrument Characteristics

- Selected for flight on Terra (launched Dec. 1999) and Aqua.
- Medium-resolution, multi-spectral, cross-track scanning radiometer.
- Measures physical properties of the atmosphere, and biological and physical properties of the oceans and land.
- 36 spectral bands—21 within 0.4-3.0 µm; 15 within 3-14.5 µm.
- Continuous global coverage every 1 to 2 days.
- Signal-to-noise ratios from 900 to 1300 for 1 km ocean color bands at 70° solar zenith angle.
- NEDT's typically < 0.05 K at 300K.
- Absolute irradiance accuracy of 5% for <3 µm and 1% for >3 µm.
- Daylight reflection and day/night emission spectral imaging.

Table 3 Instrument Facts of MODIS

Responsible Center:	NASA Goddard Space Flight Center

Heritage:	Advanced Very High-Resolution Radiometer (AVHRR), High Resolution Infrared Radiation Sounder (HIRS), Landsat Thematic Mapper (TM), and Nimbus-7 Coastal Zone Color Scanner (CZCS)
Polarization Sensitivity:	2% from 0.43 µm to 2.2 µm and ±45° scan
Swath:	2300 km at 110° (±55°) from 705 km altitude
Mass:	229 kg
Duty Cycle:	100%
Data Rate:	6.2 Mbps (average), 10.5 Mbps (day), 3.2 Mbps (night)
Thermal Control By:	Radiator
Thermal Operating Range:	268°K ±5°K
Field of View (FOV):	±49.5°
Instrument Instantaneous FOV:	250 m (2 bands), 500 m (5 bands), 1000 m (29 bands)
Geolocation (100m, 2σ)	
Control:	3600 arcsec
Knowledge:	141 arcsec
Stability:	28 arcsec/sec
Jitter:	1031 arcsec/sec (yaw and roll), 47 arcsec/sec (pitch)
Physical Size:	1.44 x 1.184 x 1.638 m

2.9 WindSat

WindSat is the primary payload of the Coriolis satellite which was launched on 6 January 2003. WindSat, the first space-borne multifrequency polarimetric microwave radiometer, has been developed by the US Naval Research Laboratory (NRL) to demonstrate that ocean surface wind vectors can be derived from space using a passive instrument. The resolution of the winds is defined by the lowest frequency channel. Although not a scatterometer, it is useful for monitoring purposes to treat it as such due to the ambiguity present in the wind vectors.

The WindSat radiometer is well-calibrated and contains the lower frequency channels required for SST retrievals. The radiometer operates in 5 discrete channels: 6.8, 10.7, 18.7, 23.8 and 37.0 GHz. All are fully polarimetric except the 6.8 and 23.8 GHz channels that have only dual polarization. Table 4 summarizes the channel details. The feedhorns of each frequency channel

trace out different arcs along the scan, therefore the Earth Incidence Angles (EIA) are different for each frequency band. Unlike previous radiometers, the WindSat sensor takes observations during both the forward and aft looking scans. This makes the WindSat geometry of the earth view swath quite different and significantly more complicated to work with than the other passive microwave sensors. The RSS WindSat products are the only dataset available that uses both the fore and aft look directions. By using both directions, we obtain a wider swath and more complicated swath geometry as is visible in the browse images (Gaiser et al., 2004).

Table 4 Summary of WindSat channels, polarizations Earth incidence angles and channel resolutions. Polarizations are listed as V for Vertical, H for Horizontal, P for +45 deg, L for Left Circular, and R for Right Circular (Wentz, F.J., L.Ricciardulli, C.Gentemann, T. Meissner, K.A. Hilburn, 2013)

Band [GHz]	Polarizations	Average EIA [deg]	Spatial Resolution (3-dB footprint size) [km x km]
6.8	V, H	53.8	39 x 71
10.7	V, H, P, M, L, R	50.1	25 x 38
18.7	V, H, P, M, L, R	55.6	16 x 27
23.8	V, H	53.2	20 x 30
37.0	V, H, P, M, L, R	53.2	8 x 13

2.10 Bay of Bengal (BoB)

Bay of Bengal a northern extended arm of the Indian ocean, is located between latitudes 20°N and 23°N and longitudes 88°E and 93°E. It is bounded in the west by the east coasts of Sri Lanka and India, on the north by the deltaic region of the Ganges-Brahmaputra-Meghna river system, and on the east by the Myanmar peninsula extended up to the Andaman-Nicobar ridges (Banglapedia, 2014). The recent two verdicts of maritime boundary of Bangladesh with Myanmar and India, allowed the country to exercise sovereign right to 118,813 sq. km of waters extending up to 12 nautical miles of territorial sea and a further Exclusive Economic Zone (EEZ) of 200 nautical miles into the sea and continental shelf extending up to 354 nm from the Chittagong coast (Hussain et al., 2017). This award allowed Bangladesh to establish sovereign rights over the living and non-living resources of BoB territorial waters. Fig. 1 shows the present maritime boundary of Bangladesh.

The BoB is featured with a humid monsoon climate with moderate rainfall 1638-3558 mm and air temperatures 19-33° C prevail in the coastal belt. SST varies from 22.8-32.9° C in the BoB. The surface salinity varies from 10-29 ppt and increases rapidly within the upper depth of 20-30 m. The primary productivity of BoB is very rich during the northeast monsoon (NEM), 0.15-1.45cm^2 day^{-1}.

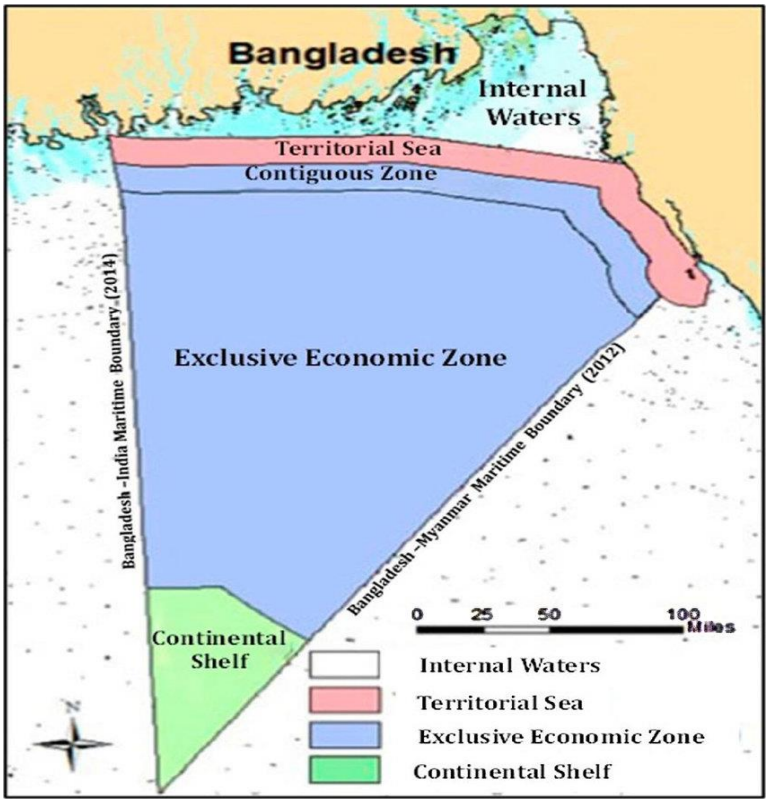

Fig. 2 Maritime area of Bangladesh (MoFA 2014)

2.11 Seasons of Bangladesh

Bangladesh has a subtropical seasonal monsoon, characterized by wide seasonal variations in rainfall, moderately warm temperatures, and high humidity. Based on monsoon, four seasons are recognized such as pre-monsoon (March, April, and May), southwest monsoon (June to September), post-monsoon (October and November) and northeast monsoon or winter (December, January, and February). Southwest monsoon is the most important feature of controlling the climate of Bangladesh. More than 71% of the annual rainfall is received during this season. Variability in the onset, withdrawal of monsoon and rainfall during the monsoon season has profound impacts on fisheries, water resources, power, agriculture, and ecosystems, in Bangladesh. On the other hand, in the winter season, the temperature falls and causing a decrease in SST. The brief characteristics of four seasons are given below:

Winter or Northeast Monsoon (December - February)

This season is characterized by very light northerly winds, mild temperature, dry weather, and lower SST. It is also known as the winter season. The mean temperature is in the range of 18-22° C and SST 24-26.7° C. Only 2% of the annual total rainfall occurs in this season (Khatun et al. 2016). During winter season, the northeasterly winds prevail over the country blowing from land to sea except northern hilly areas where mainly easterly wind prevails. But during the passage of upper air cyclonic circulation over northwestern part of the country (called western disturbances) light rain occurs over the country (Khatun et al., 2016).

Summer or Pre-Monsoon (March-May)

The mean temperature of Bangladesh during the summer months varies between 23-30 °C and SST 26.50-30.80 °C. April and May are the hottest months of a year. The highest maximum temperature ranging from 36-40^{o}C is attained in the northwestern and southwestern districts. Low-pressure results in the formation of thunder cloud and the development of severe thunderstorms. Only 19 % of the total annual rainfall occurs in this season. This season is also characterized by cyclogenesis in the BoB. Some of the low pressure formed over the BoB intensified into a depression and turned into a cyclonic storm. They are occasionally associated with storm surges and causes of high causalities and damages. Thunderstorms are very common during this season over the country. In this season, localized thunderstorms associated with violent winds, torrential downpours and occasionally hail occur. These are locally known as the 'Kalbaishakhi' are the common weather phenomena (Khatun et al., 2016).

Southwest Monsoon (June - September)

In this season, the surface wind changes to southwesterly/southerly direction. Wind speed remains light to moderate. The onset and withdrawal of monsoon vary from year to year and place to place. SST is ranged from 28 to 30.50° C. In general, rain with widespread cloud coverage and high humidity are the characteristics of this season. More than 71 % of the total annual rainfall occurs in this season. Monsoon depression forms over the BoB during this season. They generally move northwestwards and cross the Indian coast. Some of them move towards Bangladesh coasts and caused heavy rainfall. Depressions seldom attain into cyclone state in this season (Khatun et al., 2016).

Post-Monsoon (October - November)

This is the transitional season from summer monsoon to the winter. Rainfall decreases considerably during October and November. Only 8% of the annual total rainfall occurs in this season (Khatun et al., 2016). Temperature falls noticeably. SST is ranged from 27.50 to 30.50°C. Cyclonic disturbances from over the BoB during this season (Khatun et al., 2016).

2.12 Satellite imagery

POC in coastal margin environments typically occurs in complex systems where most features vary dramatically in time and space. Over short timescales (e.g., hours to days), this variability limits the utility of shipboard in situ measurements for mapping the spatial concentration and flux of materials in coastal margins. Although data obtained from satellites can provide some of the routine, synoptic information required to study these complex environments, commensurate shipboard measurements are frequently needed to translate remote-sensing imagery to meaningful biogeochemical parameters and to facilitate process-based studies. In addition, remote sensing affords the ability to extend potentially locally derived information to regional and global scales (Bianchi and Bauer, 2012).

Ocean color is the primal facet in ocean monitoring as it is the basis for several other forms of detection. Ocean color is strongly influenced by adsorption and reflection or scattering of light at the water's surface. Light in the red wavelengths is strongly absorbed by uncontaminated water, making the oceans appear blue. Some of this blue light is reflected and can be used by remote sensors to categorize targets. Particles or objects will scatter the light enabling these to be detected. This is the basis of much of the work that has been using ocean color. Further, any applications of the use of color must be subject to certain criteria to enable its use for certain facets of environmental studies, and several researchers have studied the oceans and mapped out areas where sensor calibrations can suitably be conducted (Fingas, 2018) .

2.13 Remote sensing

Remote sensing (RS) is an art or science of telling something about an object without touching it. Remote sensing of the marine environment began in the mid-20th century with the use of cameras and acoustic sensors to characterize the target. This has grown to satellites dedicated to the task of delineating various aspects of the marine environment. RS collect data by detecting the energy level that is reflected from Earth. Radiation that is emitted or reflected by the object or water body, is recorded by sensors. These sensors can be on satellites or mounted

on aircraft (NOAA 2017). Light from the sun reflects on the water body and directed satellite sensors (passive RS). At that time, the possible interactions are absorption and scattering by the water constituents; reflection, and absorption by the sea surface; reflection and refraction at the water/air interface; and absorption and scattering the atmosphere (Fig. 3). The success of the applications of RS is improved considerably by taking a multiple view approach to data collection i.e. data can be taken either by multistage sensing (data about a site are collected from multiple altitudes) or multispectral sensing (data are acquired simultaneously in several spectral bands) or multi- temporal sensing (data are collected on more than one occasion).

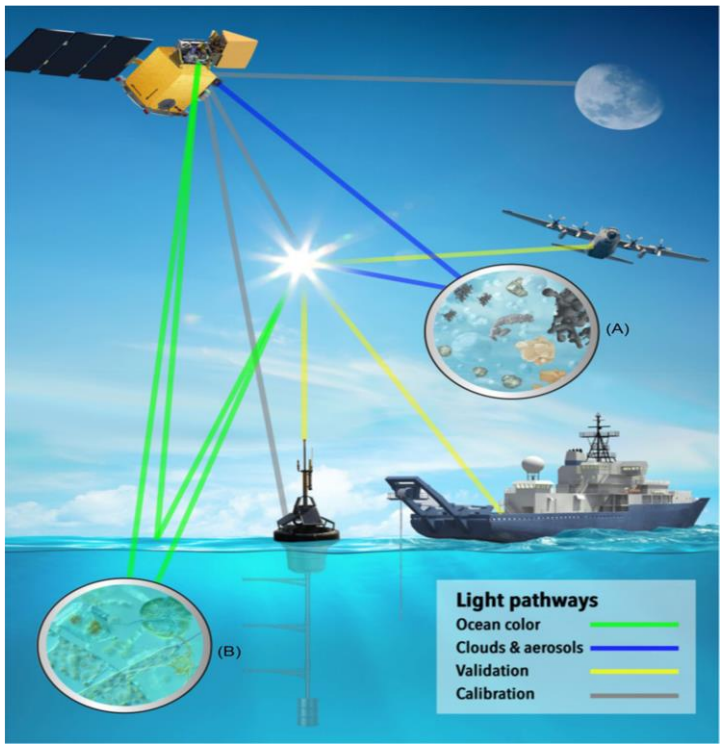

Fig. 3 Depiction of various sensor, atmospheric, and oceanic optical pathways relevant to satellite ocean color data processing (Jeremy Werdell and McClain, 2019)

Ocean color

Ocean color is the primal facet in ocean monitoring as it is the basis for several other forms of detection. Ocean color is strongly influenced by adsorption and reflection or scattering of light at the water's surface. Light in the red wavelengths is strongly absorbed by uncontaminated water, making the oceans appear blue. Some of this blue light is reflected and can be used by remote sensors to categorize targets. Particles or objects will scatter the light enabling these to be detected. This is the basis of much of the work that has been using ocean color. The goal of satellite ocean color analysis is to accurately estimate the water-leaving radiance spectra in order to derive other geophysical and optical quantities from those spectra, for example, the

concentration of the photosynthetic pigment chlorophyll-a and metrics for light penetration (Jeremy Werdell and McClain, 2019). Further, any applications of the use of color must be subject to certain criteria to enable its use for certain facets of environmental studies, and several researchers have studied the oceans and mapped out areas where sensor calibrations can suitably be conducted (Zibordi and Mélin, 2017). Among them, MODIS is commonly now commonly used to measure global POC concentration.

3. Materials and Methods

3.1 Study area

Study area for the research is the Bay of Bengal (latitude: 16.68-23°N, longitude: 88.56-93°E) which has a depth extended up to approximately 200- 4000 m (Fig. 4).

3.2 Data set

In this study, monthly average MODIS Aqua POC ,Chl-a, and SST (11µm daytime) were derived from the ocean color web of NASA (National Aeronautics and Space Administration) (https://oceancolor.gsfc.nasa.gov) from July 2002 to December 2019. Gridded monthly wind data were collected from the WindSat Polarimetric Radiometer satellite that has 5 discrete bands of Asia Asia-Pacific Data Research Center (APDRC) of NOAA (National Oceanic and Atmospheric Administration) (http://apdrc.soest.hawaii.edu/) from January 2003 to December 2019 (Table 5).

Bangladesh is in the sub-tropical monsoon climate regime. Based on the considered climate of this country (Khatun et al., 2016), four seasons are recognized as- pre-monsoon (March, April and May), southwest monsoon (June to September), post-monsoon (October and November) and northeast monsoon (December, January and February) in this study.

3.3 Data properties

The output unit of particulate organic carbon (POC) is mgm^{-3}, calculated using an empirical relationship derived from in situ measurements of POC and blue-to-green band ratios of remote sensing reflectance's (*Rrs*) on the availability of bands centered at 443 nm in the blue region and between 547 and 565 nm in the green region (Stramski et al., 2008).

The algorithm is a power law relationship between a ratio of *Rrs* and *POC*:

$$POC = a \times \left(\frac{Rrs(443)}{Rrs\ (553)}\right)^{b}$$

Where,

a=203.2

b=−1.034

Relationships between the surface concentration of particulate organic carbon and optical properties are discussed detail by (Stramski et al., 2008).

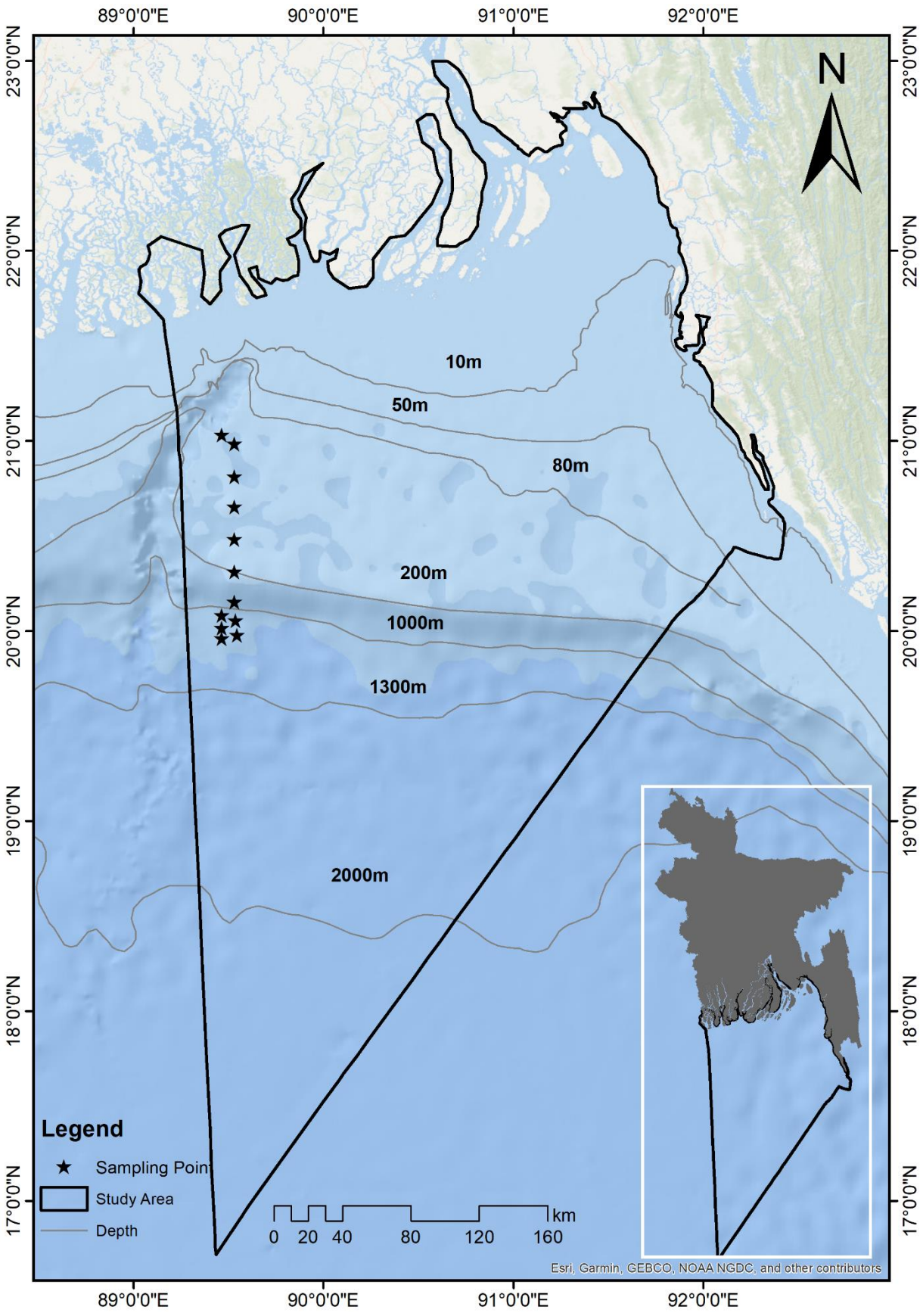

Fig. 4 Study area map and in-situ sampling points in the BoB

The output unit of the Chl-a value is mgm^{-3}. The Chl-a product combines two algorithms, the O'Reilly band ratio OCx (e.g. chl_oc4) algorithm and the Hu color index (CI)algorithm (chl_hu). For Chl-a retrievals below 0.15 mgm^{-3}, the color index (CI) algorithm is used. For Chl- a retrievals above 0.2 mgm^{-3}, the OCx algorithm is used. In between these values, the CI and OCx algorithm are blended using a weighted approach (NASA, 2014a).

Sea surface temperature (SST) in units of °C (degree Celsius) using the 11um and 12um long wave infrared bands. The algorithm is based on a modified version of the nonlinear SST algorithm of Walton et al., (1998) and is applicable to both MODIS and VIIRS sensors for daytime and nighttime observations (NASA, 2014b). Here, daytime 11 um data were used to analyze SST value.

In case of monthly wind vector data (2003-2019), 10-meter surface wind speed - all weather (m/s) and 10-meter surface wind direction- relative to north (deg) were taken for the investigation of wind on POC image seasonally. Detail data properties are presented in Table 5.

Table 5 Data properties

Data type	Sensor	From-date	Interval	Number of data
POC	MODIS Aqua	July 2002 - December 2019	Monthly	222
Chl-a	MODIS Aqua	July 2002 - December 2019	Monthly	222
SST	MODIS Aqua	July 2002 - December 2019	Monthly	222
Wind	WindSat	January 2003 - December 2019	Monthly	204

3.4 Data Processing:

POC, Chl-a and SST data were analyzed by satellite image processing software SeaDAS 7.5.3, which is mainly used to process different level (1, 2 or 3) ocean color data. This software is capable to rasterize the standard mapped image (SMI) level-3 satellite image. After rasterization, the image was cropped according to our study area and obtained the statistical information (maximum value, minimum value, mean, median, standard deviation etc.) using 'Display Statistics' tool. Detail flow chart for the MODIS Aqua data processing are shown in Fig. 5.

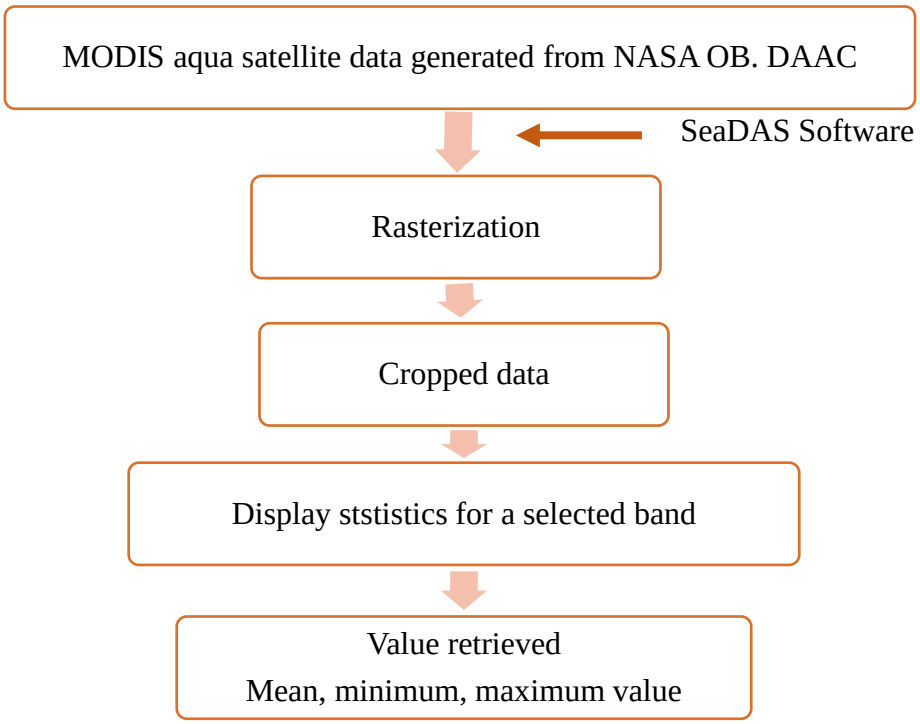

Fig. 5 Flow chart of the MODIS Aqua satellite image processing

WindSat data were analyzed using ArcGIS 10.4 Software which processes the raster images of wind speed and direction into vector form by 'Make netCDF Feature Layer' of 'Multidimensional tools'. After the vector data formation, the layer properties of the data in the study area were symbolized by arrow sign. Then the monthly POC data were opened in ArcGIS 10.4 and cropped the selected study area (BoB) by the tool of 'Extract by mask' and overlapped on the POC image. Detail flow chart for the WindSat processing are shown in Fig. 6

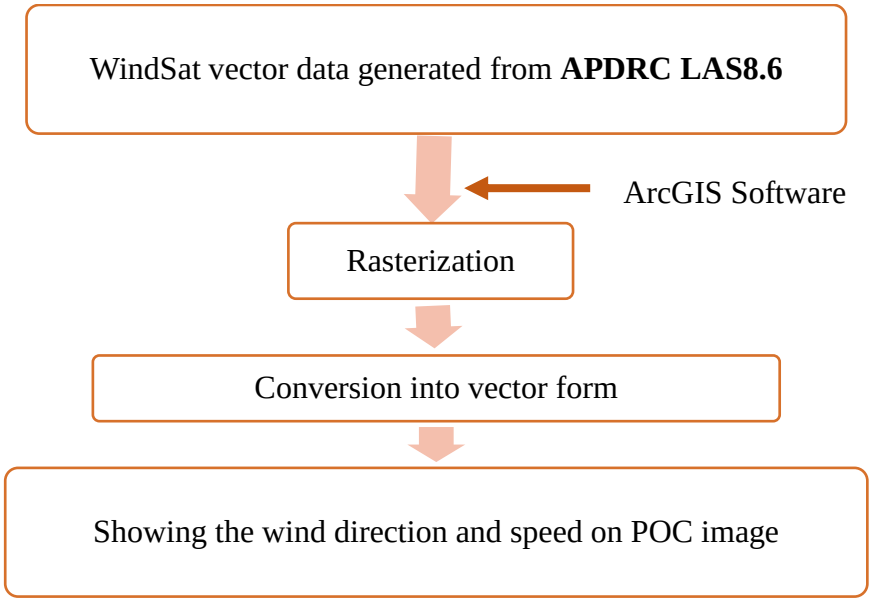

Fig. 6 Flow chart of the WindSat Satellite image processing

3.5 In-situ measurement:

In-situ POC was estimated following the method prescribed by Parsons et al., (1984). Special apparatus and equipment and regents are listed in **Annex I**.

Sample collection: Samples were collected from twelve different sampling stations from latitude 20°00'37.32" N to 21° 10'8" N along about 89° 28' E to 89° 32' longitude with a 3' (3 min) geographic coordinate (Fig. 1) interval on 2,6 December, 2019 during daytime (8 am-3.30 pm) with BNS Turag, a Ship of Bangladesh Navy. Water samples were collected using non-toxic opaque sampler from the depth of 0.5 m and stored in opaque bottles (1-liter high-density polyethylene sample bottles).

Filtration: Filtration was carried out within one hour of collection of the sample with a vacuum pump. Nitrocellulose filter of 47 mm diameter and 0.45 µm pore size was used. After filtration of a suitable sample of seawater (usually 0.5 L), full suction to the filter was applied. Releasing the suction after 1 min, 2 ml of sodium sulfate reagent was added, and it was reapplied the suction immediately by adding 2 ml of sodium sulfate once again and the filter under suction was removed. Filtration volume was recorded for each filter and after filtration, filter papers were folded half and wrap in prelabeled aluminum foil and placed in a freezer. The samples were then shifted to the water quality laboratory of Fisheries and Marine Resource Technology Discipline of Khulna University. The laboratory analysis for estimating POC is described below:

- Placing the filter in a 30-ml beaker and pressed it into the bottom. 1.0 ml of phosphoric acid and 1.0 ml of distilled water were added. Then it was mixed and placed in a hot plate at 100°C for 30 min and covered with a watch glass during this period.
- 10 ml sulfuric acid-dichromate oxidant and 2 ml distilled water were added.
- Then the solution was mixed by swirling and placed a cover glass over each beaker. And again, it was placed in a hot plate for 60 min at 100°C.
- Cooling the mixture, the solution and glass fiber filter were transferred to a suitably sized graduated cylinder. The sides of the beaker were rinsed with distilled water and the graduated cylinder was made up to volume with distilled water. Stopper and mixed by inverting; allowing to stand at room temperature to cool and to allow the filter to settle in the bottom of the cylinder.
- The extinction of a blank solution against the sample at 440 nm using a 1cm cuvette path length was measured.

- The resulting extinction for the absorbance of trivalent chromium was corrected by the expression:

$$E = 1.1 * E_f$$

Where,

E= Extinction for trivalent chromium

E_f= Extinction difference sample and blank solution.

Finally, POC in mgm^{-3} was estimated using the following formula:

$$POC\ (\mu g/l) = \frac{E*F*v}{V}$$

Where,

F= Calibration factor = 275

V= volume of seawater filtered in liters

v= volume of oxidant

3.6 Data analysis

All statistical analyses including correlation, regression, one-way ANOVA and post-hoc test was performed using R- studio and SPSS.

4. Result

4.1 Seasonal trend of particulate organic carbon (POC) concentration in BoB

BoB has a unique character called monsoon that demarcates the season and influences the major phenomena of the sea part as well as the territorial part of Bangladesh. Therefore, monsoon has a major influence on POC variability over the BoB. So, understanding the seasonal POC variability helps us to reveal the effects of monsoon on POC variability. The seasonal pattern of POC in the BoB is illustrated by climatological monthly composites of the MODIS-aqua images from July 2002 to June 2019 (Fig. 7). In this Figure, a month represents the average value of the same month for all the years from 2002 to 2019. Monthly averaged POC was ranged between 103.08 and 184.22 mgm^{-3}. Northeast-monsoon (December-February) showed the highest (181.80 ±22.34 mgm^{-3}) POC. From that, a small reduced concentration was observed during two monsoon seasons, i.e., post-monsoon (October-November) (162.33±28.16 mgm^{-3}) and Southwest Monsoon (June- September) (141.31 ±36.40 mgm^{-3}). Lowest POC (136.56±36.24 mgm^{-3}) was found during pre-monsoon (March-May) particularly in the month of May (115.38±41.31 mgm^{-3}) (Fig. 6).

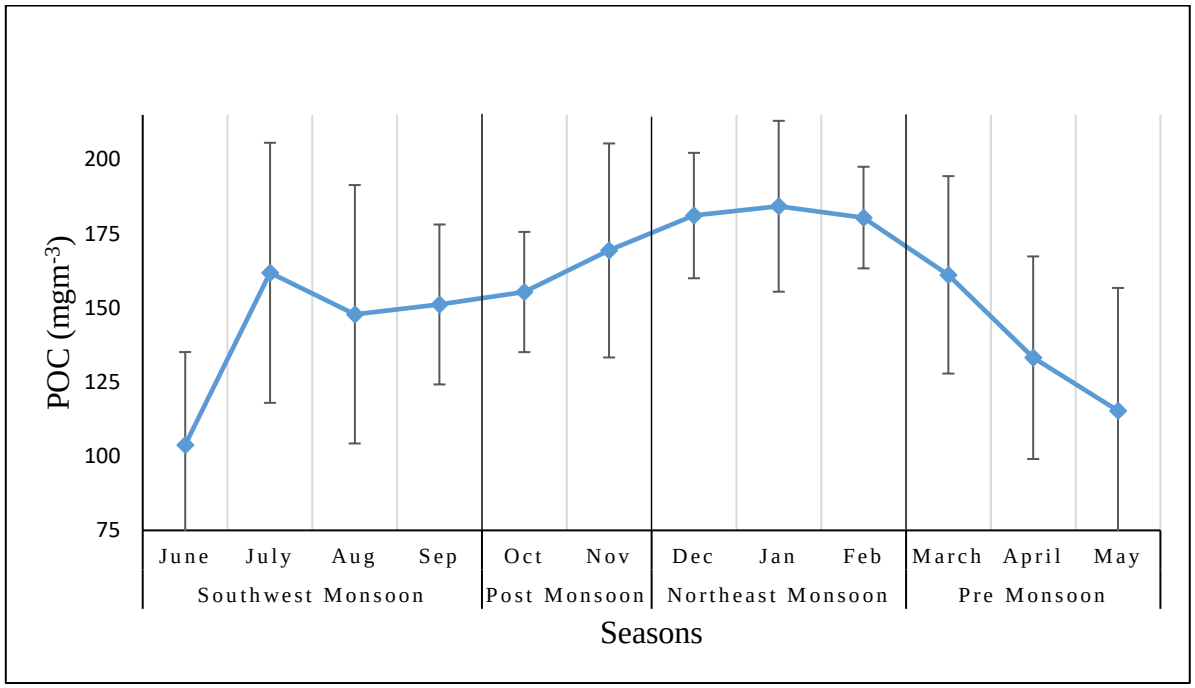

Fig. 7 Seasonal distribution of POC with the monthly climatological average from 2002 to 2019

POC was found significantly different ($F_{(3,202)} = 18.09$, $p = .000$) among the seasons according to the analysis of one-way ANOVA (Table 6). The post hoc analysis (LSD) also showed significant difference among the seasons except the mean difference between the southwest and pre monsoon ($p = .433$) (Table 7).

Table 6 Statistical test for variability of mean POC among the seasons.

ANOVA

POC

	Sum of Squares	df	Mean Square	F	Sig.
Between Groups	69937.270	3	23312.423	18.092	0.000
Within Groups	260285.894	202	1288.544		
Total	330223.164	205			

Table 7 Statistical test for multiple comparisons of POC based on season.

Multiple Comparisons

POC Least Significance Differences

(I) Seasons	(J) Seasons	Mean Difference (I-J)	Std. Error	Sig.	95% Confidence Interval	
					Lower Bound	Upper Bound
Northeast monsoon	Southwest Monsoon	40.12230*	6.64942	.000	27.0111	53.2335
	Pre-Monsoon	45.34670*	7.10853	.000	31.3303	59.3631
	Post Monsoon	16.57801*	7.81399	.035	1.1706	31.9855
Southwest Monsoon	Northeast monsoon	-40.12230*	6.64942	.000	-53.2335	-27.0111
	Pre-Monsoon	5.22440	6.64942	.433	-7.8868	18.3356
	Post Monsoon	-23.54429*	7.39879	.002	-38.1331	-8.9555
Pre-Monsoon	Northeast monsoon	-45.34670*	7.10853	.000	-59.3631	-31.3303
	Southwest Monsoon	-5.22440	6.64942	.433	-18.3356	7.8868
	Post Monsoon	-28.76869*	7.81399	.000	-44.1761	-13.3612
Post Monsoon	Northeast monsoon	-16.57801*	7.81399	.035	-31.9855	-1.1706
	Southwest Monsoon	23.54429*	7.39879	.002	8.9555	38.1331
	Pre-Monsoon	28.76869*	7.81399	.000	13.3612	44.1761

*. The mean difference is significant at the 0.05 level.

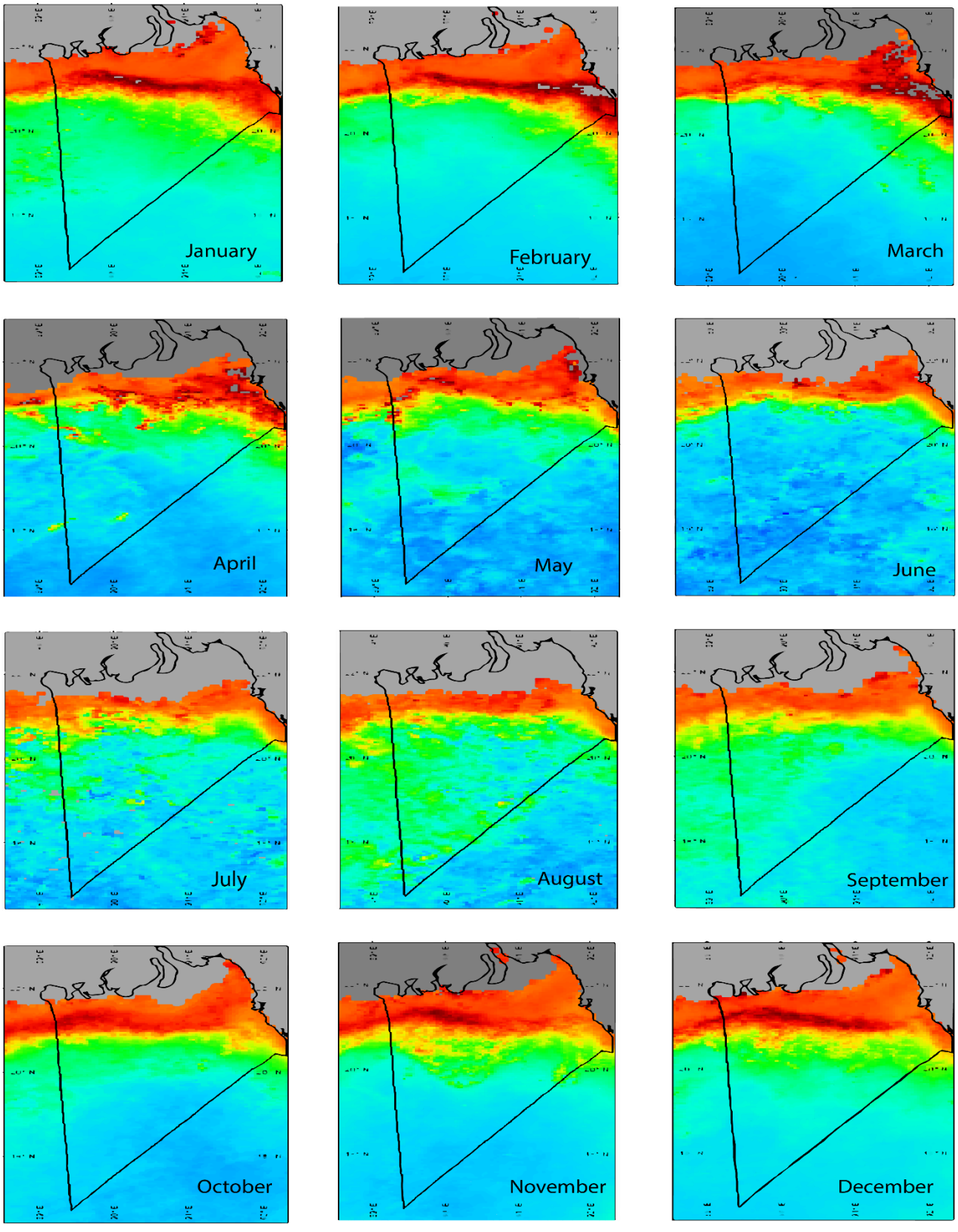

Fig. 8 MODIS derived monthly climatology of POC from July 2002 to June 2019 in the BoB.

4.2 Seasonal relation between SST and POC

SST was ranged from 24.02 ^{0}C to 30.83 ^{0}C (2002-2019) among the seasons in the study area. An inverse relation was found between SST and POC for all the seasons in the BoB. The regression coefficient (b) between SST and POC was high (-15.86) in Southwest Monsoon (June- September) and low (-6.81) in northeast-monsoon (December-February) (Fig. 8). Statistically significant relation between SST and POC was found in southwest monsoon and pre-monsoon (p<0.05) whereas no significant (p >0.05) relation was found in northeast monsoon and post-monsoon. The correlation coefficient (r) was ranged from -0.21 to -0.40 (Fig. 8).

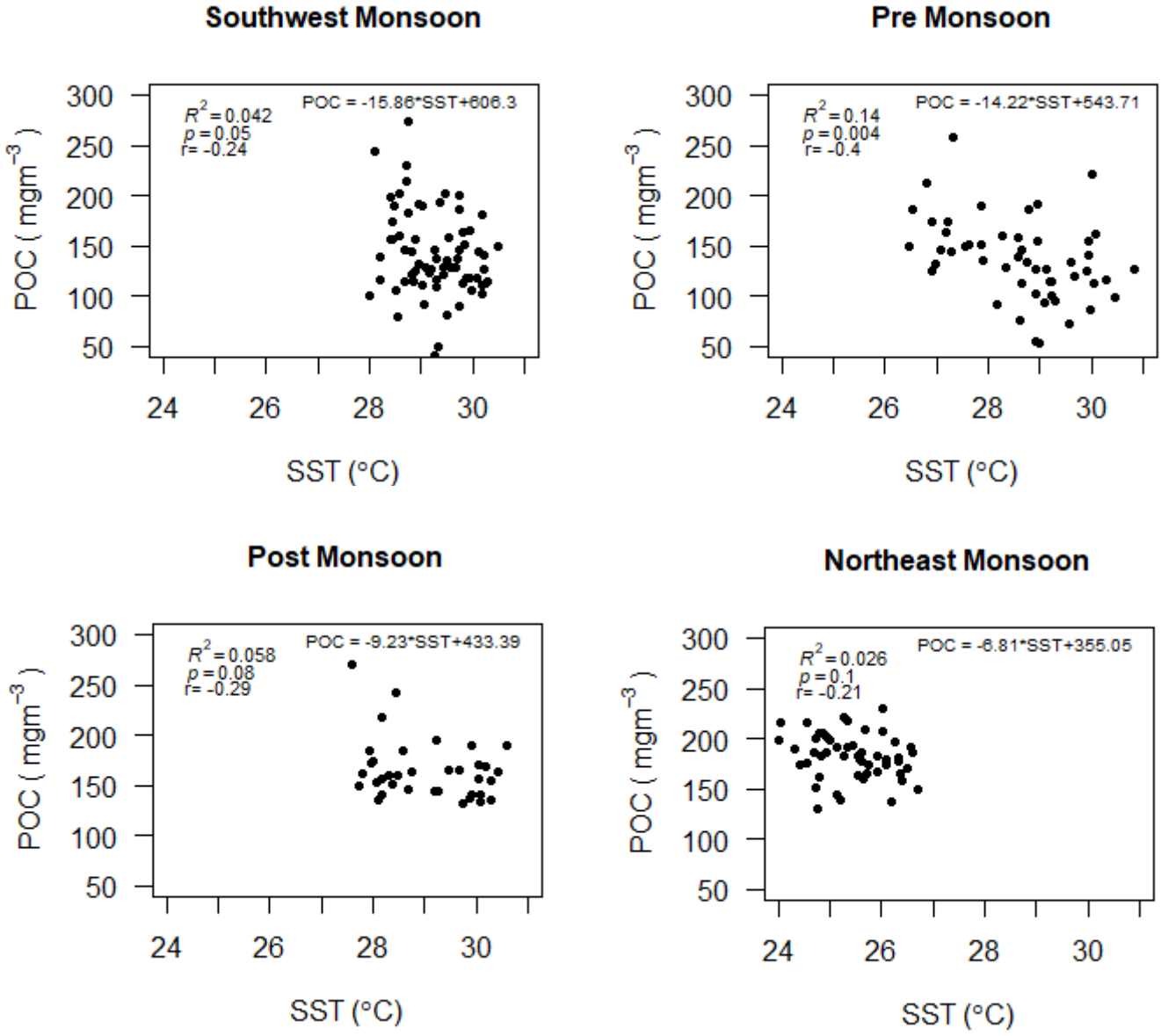

Fig. 9 MODIS derived Seasonal relationship between SST and POC from July 2002 to June 2019

4.3 Seasonal relation between Chl-a and POC

Chl-a was ranged from 0.19 to 1.94 mgm^{-3} among all the seasons (2002-2019). A strong positive relation was found between Chl-a and POC for all the seasons in the BoB. The regression coefficient (b) between Chl-a and POC was highest (78.01) in northeast-monsoon (December-February) and lowest (40.68) in pre-monsoon (March-May) (Fig. 9). Statistically significant (p<0.05) relation between the Chl-a and POC was found in all the seasons. The correlation coefficient (r) was ranged from 0.64 to 0.87 (Fig. 9).

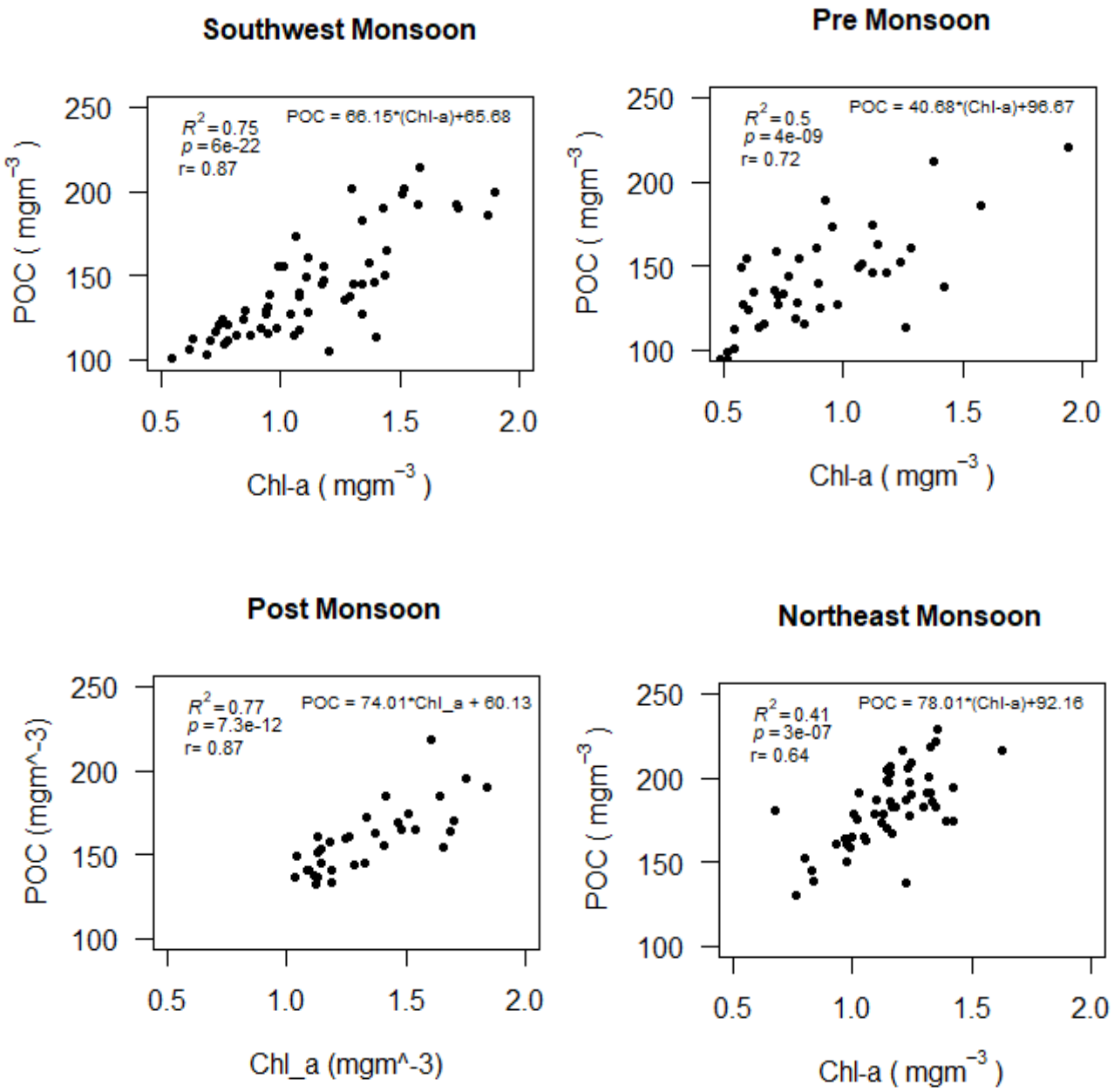

Fig. 10 MODIS derived Seasonal relationship between Chl-a and POC from July 2002 to June 2019

4.4 Seasonal realtion between POC and wind vector

A very weak positive relation was found between wind speed and POC for the Southwest Monsoon (June- September) and northeast monsoon (December-February) and a weak negative relation was found in pre and post monsoon in the BoB. The regression coefficient (b) between wind speed and POC were 4.11, 1.63, -7.51 and -7.4 in southwest monsoon (July-September), Northeast monsoon (December-February), pre and post monsoon respectively (Fig. 10). Statistically significant relation was not found between the wind speed and POC (p>0.05) in the study area.

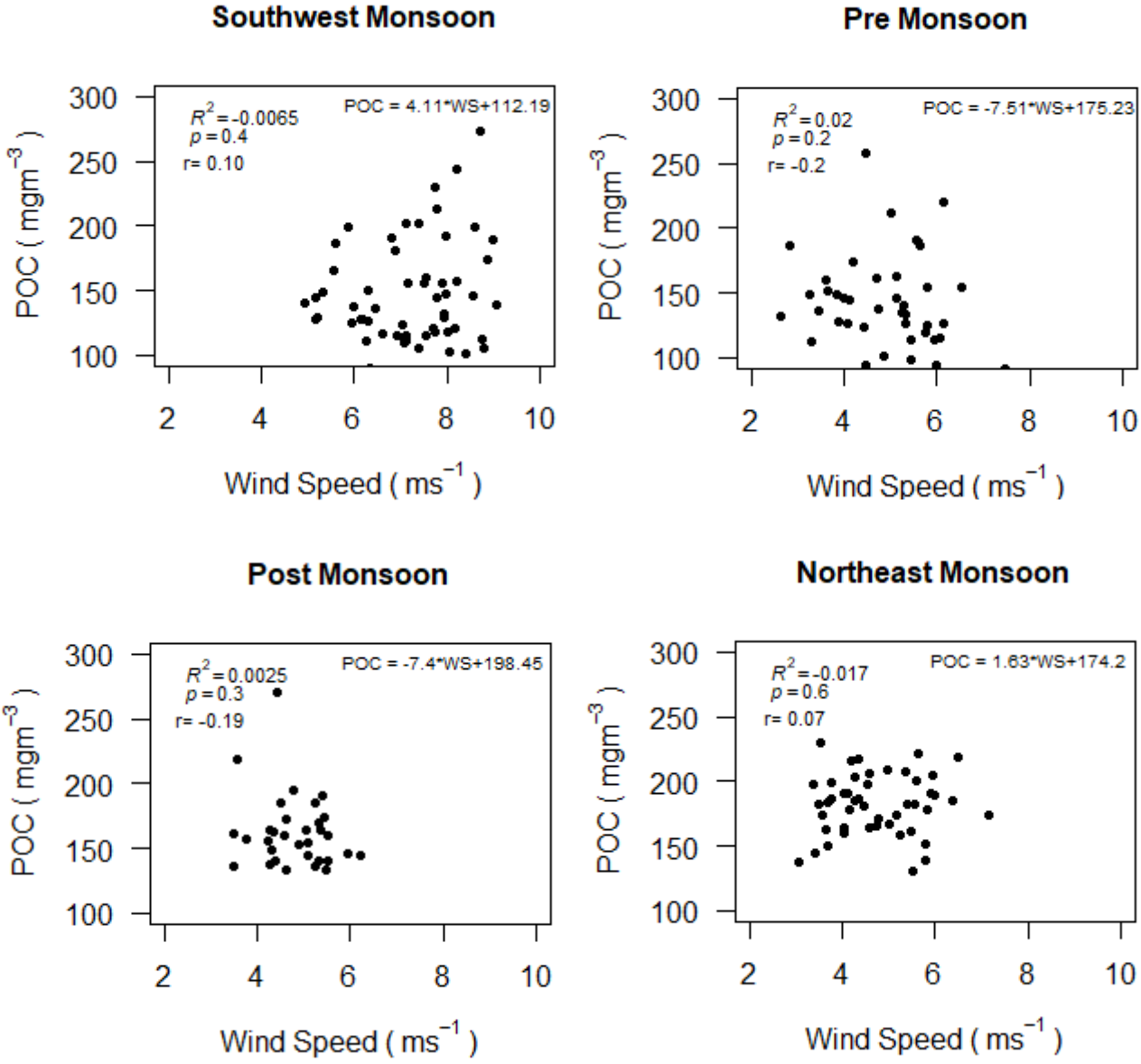

**WS= Wind Speed*

Fig. 11 WindSat derived Seasonal relationship between wind speed and POC from July 2003 to June 2019

Monthly wind speed range was 3.8-9.0 ms^{-1} in January representing northeast monsoon, 5.0-10.6 ms^{-1} in May,7.6-13.4 ms^{-1} in July and 3.6-10.0 ms^{-1} in October representing pre-monsoon, southwest monsoon and post monsoon respectively. POC was very high with the wind vectors prevailing northeasterly wind in northeast monsoon (January 2019) and post monsoon (October 2019) compared to other seasons. In southwest monsoon (July 2019) and pre-monsoon (May 2019), prevailing southwesterly winds in may have contributed to low POC in the inner, middle and outer shelves. The circulation winds October of post monsoon may have contributed to high POC in the inner shelves of the BoB (Fig. 11).

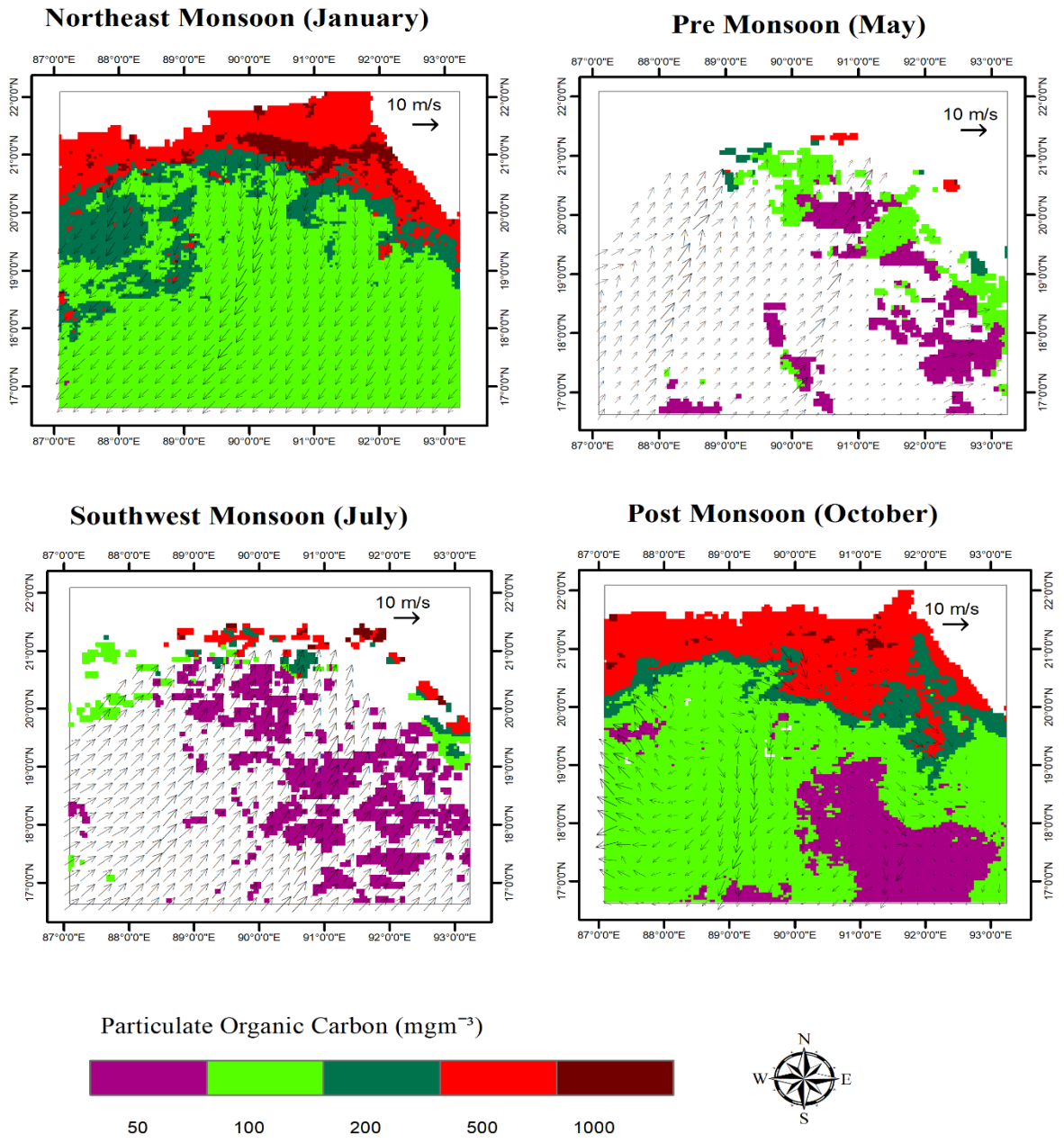

Fig. 12 WindSat derived Seasonal relationship between POC and wind vector in 2019

4.5 In-situ validation

In-situ POC measurement ranged from 62.92 to 162.14 mgm^{-3} and are shown in Table 8. The correlation coefficient (Fig. 12) between the in-situ value and MODIS-Aqua satellite-derived POC was 0.74 with a root mean square error (RMSE) of 38.15% and mean relative error (MRE) of 32.17 % (Fig. 12). The coefficient was found highly significant (p<0.05) in the study area.

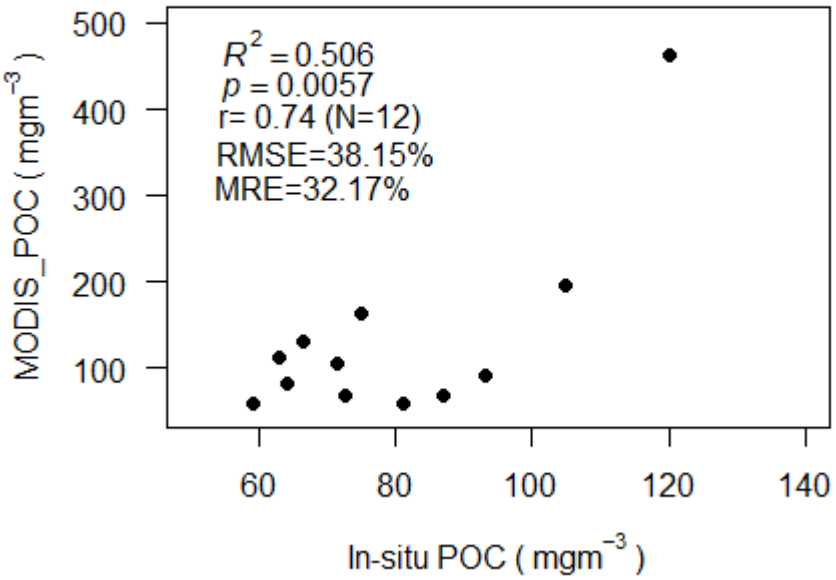

Fig. 13 Comparison of in-situ and MODIS derived POC

4.6 Relation with distance

A negative relation (-0.18) between the in-situ POC and distance with depth was found in the study area (Fig. 14). Statistically significant relation was not found between distance with depth and in-situ POC. POC was found decreasing from the shelf zone to the deep ocean (Table 8).

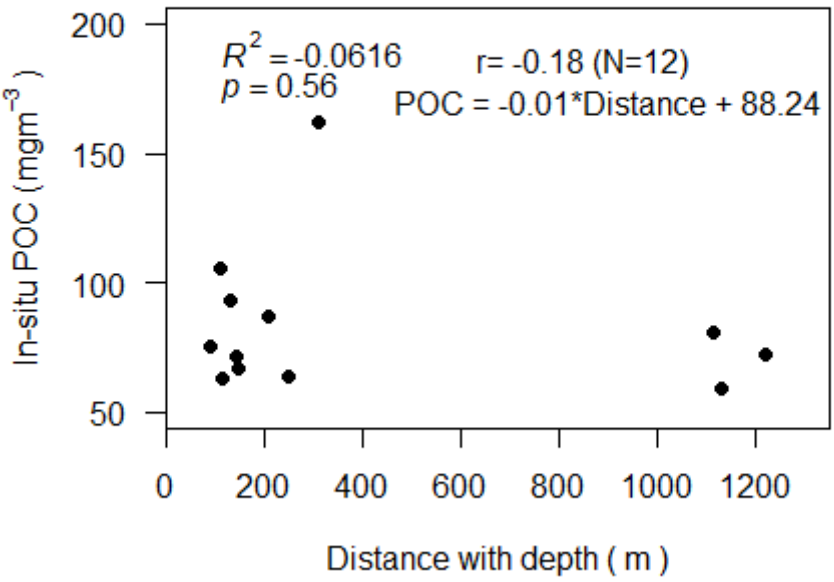

Fig. 14 Distance with depth of in-situ POC

Table 8 Sampling points and their respective values:

Date	Sampling point	Latitude	Longitude	In-situ POC value (mgm^{-3})	MODIS derived POC (mgm^{-3})	Depth (m)
02-12-19	S_1	20.00	89.47	72.6	68.69	1221
	S_2	20.02	89.47	81.07	58	1112
	S_3	20.03	89.47	87.12	69	208
	S_4	20.05	89.47	93.17	92	133
	S_5	20.08	89.47	105.27	195	110
	S_6	21.03	89.47	162.14	462	311
06-12-19	S_7	20.98	89.53	75.02	164	92
	S_8	20.81	89.53	62.92	113	115
	S_9	20.65	89.53	66.55	132	150
	S_{10}	20.48	89.53	71.39	105	144
	S_{11}	20.31	89.53	64.13	81	250
	S_{12}	20.15	89.53	59.29	60	1130

5. Discussion

5.1 Seasonal trend of POC

The surface concentrations of POC varied from 103.08 to 184.22 mgm^{-3} in the northern BoB (Fig. 6). Fernandes et al. (2009) also observed the concentration of POC from 51.6 to 133.2 mgm^{-3} in the BoB. The observed seasonal differences in POC appears to be governed by river run-off and physical forces such as eddies which pump nutrients into the surface waters thereby enhancing biological production (Fernandes et al., 2009). The seasonal variability of POC was significant in the northern BoB in this study. Fernandes et al., (2009) also observed the significant difference of POC variability among the seasons in both offshore and near stations of the BoB due to nutrient addition by organic matter production. Similar result was found by Allison et al., (2010) in the southern ocean.

5.1.1 Southwest monsoon (June – September)

Among the seasons, reasonably low POC was observed in this season (141.31 ±36.40 mgm^{-3}). Highest SST was recorded (30.58 ^{0}C) at the beginning of this seasons and responsible for this lower POC. Insufficient freshwater influx can also be a major cause for the lower range of POC (Nagamani et al., 2011). As surface water warms because of high SST, the stratification being pronounced, mixing is suppressed, and transfer of nutrients is decreased from deeper to surface waters. Therefore, phytoplankton productivity declines and POC becomes low (Stramska and Bialogrodzka, 2016). In southwest monsoon, prevailing southwesterly winds may have contributed to low POC in the inner, middle and outer shelves. Similar observation was also reported by Liu et al., (2015).

5.1.2 Post Monsoon (October- November)

Beginning of post monsoon POC starts to rise (Fig. 6). Relatively high POC (162.33±28.16 mgm^{-3}) was observed in this season than the southwest monsoon because the wind forces the nutrient rich water to reach the surface for phytoplankton cells to grow (Sarangi and Devi, 2017). Gomes et al., (2000) supported the wind driven coastal upwelling and increased river runoff during the southwest monsoon increased phytoplankton biomass dramatically which cause the enhance of phytoplankton productivity during post monsoon season.

The BoB is featured with several cyclones in this season (Sarangi et al., 2008), which provide nutrient rich subsurface water to the surface, form eddies and intensify blooms (Chauhan et al., 2002; Madhu et al., 2002) and consequential roles in formation of POC.

5.1.3 Northeast Monsoon (December- February)

POC has found highest (181.80 ±22.34 mgm^{-3}) during northeast monsoon characterized by very light northeasterly winds, mild temperature, dry weather, and lower SST (24.02 ^{0}C). Phytoplankton blooms patches generally occurred in this season (December to January) and disappear in the later months over the BoB. The blooms in this season are mainly attributed to the ocean upwelling driven Ekman pumping. Sarangi and Devi (2017) observed high nitrate dispersion on a synoptic scale during December and January. This nitrate is related to upwelling and convection processes which bring up the deeper and subsurface nutrient rich water to the surface during northeast monsoon. The winter convection process which brings nutrient rich water to the surface is responsible for the enhanced biological production (Tang et al., 2010). Highest POC of the BoB is mostly derived from phytoplankton (Fernandes et al., 2009). High POC (380 ± 28.7 mgm^{-3}) was also accorded in northeast monsoon in the Yellow-Bohai sea of China (Fan et al., 2018).

5.1.4 Pre-Monsoon (March – May)

Lowest POC (136.56±36.24mg m^{-3}) was found during pre-monsoon (March-May) particularly in the month of May (115.38±41.31mg m^{-3}) in BoB (Fig. 6). The gradual increase in SST results low POC on the BoB in this season and this relation was confirmed by previous studies (Nagamani et al., 2011).This increase of SST and decrease of wind speed. Insufficient freshwater influx can also be a reason for lower POC because fresh water influx causes high productivity by making the waters of the upper layer less saline and highly stratified (Nagamani et al., 2011). Reduction of POC in pre-monsoon due to removal process or dilution was also observed by Fan et al., (2018).

5.2 Relationship between POC and SST

Recent evidence indicating that the variability of POC is negatively correlated with SST (Yu et al., 2019). An inverse relation was found between SST and POC for all the seasons in the BoB. The coefficient of regression was high (b= -15.86) in Southwest Monsoon (June-September) and low (b= -6.81) in northeast-monsoon (December-February) (6.81) (Fig. 8).

In northeast monsoon, we observed low negative coefficient. This scenario has been supported in the past by in situ observations in the Barents sea, Norway (Stramska and Bialogrodzka, 2016) and North Atlantic (Marra et al., 2015).

In contrast, in the southwest monsoon (June- September) water becomes warm in the study area. The warm sea surface temperature (SST's) and the low salinity in the Bay of Bengal lead to strong stratification of the water column, which prevents the transport of nutrient rich bottom

waters into the surface (Fernandes et al., 2009). Therefore, phytoplankton productivity declines which results a high negative correlation between SST and POC during this season.

5.3 Relationship between POC and Chl-a

Phytoplankton production is the primary or main source for POC in the open ocean surface waters (Siegel et al., 2013; Stramska, 2009; Stramski et al., 2008, 1999a; Yoder and Kennelly, 2006). Statistically a moderate positive significant relation was found between Chl-a and POC in all the seasons where the regression coefficient was ranged from 40.68 (pre-monsoon) to 78.01 (northeast monsoon). A significantly positive but relatively lower correlation coefficient (0.64–0.87) between POC and Chl-a (Fig. 9). Similar result was also found by Yu et al., (2019) in the North Pacific Ocean. Fernandes et al., (2009) also observed a fairly good significant positive relationship between POC and Chl-a was also reported by in the BoB.

Strong correlation between POC and Chl-a reveal that POC mostly derived from phytoplankton, not terrestrial organic matter to a great extent (Fernandes et al., 2009). The relation between POC and Chl-a was low (b = 40.68) in pre-monsoon, indicating that phytoplankton was relatively less dominant source of particulate carbon in these waters (Duan et al., 2014) and high (b=78.01) in northeast monsoon suggesting that POC is intensively regulated by marine phytoplankton in association with nutrient loading from riverine inputs (Liu et al., 2019a).

5.4 Relationship between POC and wind vector

Water circulation on the inner shelf is primarily driven by wind (Nowlin et al., 2005). The monthly mean POC was weakly correlated with monthly wind speed (Fig. 11) among the seasons. Similar result was found by Le et al. (2017) on the Louisiana Continental Shelf (USA). POC distribution is associated with wind direction. High POC distribution was found in northeast and post monsoon seasons when the prevailing wind was northeasterly direction. Low POC distribution was found southwest and pre-monsoon seasons when the prevailing wind was in southwesterly direction (Fig. 11). Similar pattern was reported by Liu et al., (2015).

Northeasterly winds prevail during winter, which drives westerly surface currents along the shore. In northeast monsoon, strong wind strengthens tidal currents, leading to intensive sediment resuspension. POC concentrations were positively correlated with wind speed (Liu et al., 2019a). Surface POC concentrations were high with high water velocity that were association with wind. Surface POC concentration decreased during the late period of tidal

ebbing and early period of tidal flooding with low water velocity; the same pattern was observed during the late period of tidal flooding and early period of tidal ebbing (Liu et al., 2019a).

5.5 Validation of MODIS Aqua derived POC

In-situ POC measurement ranged from 62.92 to 162.14 mgm^{-3} and are shown in Table 5. The correlation coefficient (Fig. 12) between in-situ and MODIS-Aqua satellite-derived POC was 0.74 with a root mean square error (RMSE) of 38.15% and mean relative error (MRE) of 32.17 % (Fig. 12). Lower values of RMSE indicate better fit of the of the model to the data representing how close the observed data points are to the model's predicted values (Yu et al., 2019). Le et al. (2017) observed a similar performance as on the Louisiana Continental Shelf (LCS) in USA with R^2=0.64, MRE=36.9%, and RMSE=49.8% using MODIS Aqua imagery. Duan et al. (2014) also observed a strong relationship between in-situ measured POC and MODIS estimated POC (N=16, RMSE=44.46%) using POC algorithm for the Yangtze River, China. General sources of error associated with any ocean-color product include differences introduced by choice of sensor, sensor calibration, and the atmospheric correction procedure used to retrieve remote-sensing reflectance (*Rrs*) (Evers-King et al., 2017). Further understanding of the sources of variability between POC and optical parameters can then be incorporated into future, semi-analytical algorithms. New understanding of these relationships may also inform future sensor development (e.g., hyperspectral sensors) and optical modeling technique (Evers-King et al., 2017).

5.6 Relation with distance

A negative relation (-0.18) between the in-situ POC and distance with depth was found in the study area (Fig. 14). POC was decreasing from the lower depth area i.e., shelf zone (100-300m) to the higher depth area i.e., deep ocean. Similar result was observed in Fig.8 illustrated the raster image of multiyear monthly data. Because The primary productivity of phytoplankton is negatively correlated with the depth (Stramska, 2014). The observed decrease with depth of POC indicates heterotrophic uptake and/or dilution by inorganic material which results poor POC (Fernandes et al., 2009). So, phytoplankton distribution is mainly responsible for the phenomenon in the Bay of Bengal. The euphotic depth variability was also accountable for the vertical distribution of POC (Liu et al., 2015).

6. Conclusion and recommendation

Conclusion:

- Highest POC was observed during northeast monsoon and lowest during pre-monsoons months.
- Monthly POC was inversely related to monthly SST which has almost no contribution on the variability of POC in the BoB.
- There was a positive relation between Chl-a and POC in the BoB.
- POC variability was mostly influenced by Chl-a than SST indicating Chl-a has the greatest contribution on the variation of POC.
- There was not a statistically significance difference between wind speed and POC (p>0.05).
- POC was very high with the wind vectors prevailing northeasterly wind and low with the southwesterly winds.
- There was a moderate positive relation between the in-situ value and MODIS-Aqua satellite-derived POC.
- There was a negative correlation between in-situ POC and depth in the BoB.
- POC was decreasing from the shelf zone to the deep ocean.

Recommendation:

- The spatial resolution of MODIS-Aqua satellite is very high. Low resolution data can provide more accurate estimation of POC.
- There need to generate a regional algorithm for the best measurement of POC.
- There need more facilities for more intense in-situ field measurement and need to increase the sampling number.
- Further studies are needed to address the multiple factors responsible for POC variability.

7. References

Allison, D.B., Stramski, D., Mitchell, B.G., 2010. Seasonal and interannual variability of particulate organic carbon within the Southern Ocean from satellite ocean color observations. J. Geophys. Res. 115, C06002. https://doi.org/10.1029/2009JC005347

Alongi, D.M., Boto, K.G., Tirendi, F., 1989. Effect of exported mangrove litter on bacterial productivity and dissolved organic carbon fluxes in adjacent tropical nearshore sediments. Mar. Ecol. Prog. Ser. Oldend. 56, 133–144.

Bai, Y., Cai, W.-J., He, X., Zhai, W., Pan, D., Dai, M., Yu, P., 2015. A mechanistic semi-analytical method for remotely sensing sea surface $p\,CO_2$ in river-dominated coastal oceans: A case study from the East China Sea. J. Geophys. Res. Ocean. 120, 2331–2349. https://doi.org/10.1002/2014JC010632

Bai, Y., He, X., Pan, D., Chen, C.T.A., Kang, Y., Chen, X., Cai, W.J., 2014. Summertime Changjiang River plume variation during 1998-2010. J. Geophys. Res. C Ocean. 119, 6238–6257. https://doi.org/10.1002/2014JC009866

Banglapedia, 2014. Bay Of Bengal EAFM 25–27.

Battin, T.J., Kaplan, L.A., Findlay, S., Hopkinson, C.S., Marti, E., Packman, A.I., Newbold, J.D., Sabater, F., 2008. Biophysical controls on organic carbon fluxes in fluvial networks. Nat. Geosci. 1, 95–100.

Bhosle, N.B., Dhople, V.M., Wagh, A.B., 1988. Distribution of particulate organic carbon in the central Arabian Sea. Proc. Indian Acad. Sci. - Earth Planet. Sci. 97, 35–47. https://doi.org/10.1007/BF02861625

Bianchi, T.S., 2007. Biogeochemistry of estuaries. Oxford University Press on Demand.

Bianchi, T.S., Bauer, J.E., 2012. Particulate Organic Carbon Cycling and Transformation, Treatise on Estuarine and Coastal Science. Elsevier Inc. https://doi.org/10.1016/B978-0-12-374711-2.00503-9

Bianchi, T.S., Wysocki, L.A., Stewart, M., Filley, T.R., McKee, B.A., 2007. Temporal variability in terrestrially-derived sources of particulate organic carbon in the lower Mississippi River and its upper tributaries. Geochim. Cosmochim. Acta 71, 4425–4437. https://doi.org/10.1016/j.gca.2007.07.011

Biddanda, B., Benner, R., 1997. Carbon, nitrogen, and carbohydrate fluxes during the production of particulate and dissolved organic matter by marine phytoplankton. Limnol. Oceanogr. 42, 506–518. https://doi.org/10.4319/lo.1997.42.3.0506

Boyer, J.N., Christian, R.R., Stanley, D.W., 1993. Patterns of phytoplankton primary productivity in the Neuse River estuary, North Carolina, USA. Mar. Ecol. Prog. Ser. Oldend. 97, 287–297.

Boynton, W.R., Kemp, W.M., Keefe, C.W., 1982. A comparative analysis of nutrients and other factors influencing estuarine phytoplankton production, in: Estuarine Comparisons. Elsevier, pp. 69–90.

Cahoon, L.B., 2002. The role of benthic microalgae in neritic ecosystems, in: Oceanography and Marine Biology, An Annual Review, Volume 37. CRC Press, pp. 55–94.

Chauhan, P., Mohan, M., Sarngi, R.K., Kumari, B., Nayak, S., Matondkar, S.G.P., 2002. Surface chlorophyll a estimation in the Arabian Sea using IRS-P4 Ocean Colour Monitor (OCM) satellite data. Int. J. Remote Sens. 23, 1663–1676. https://doi.org/10.1080/01431160110075866

Cheng, J., Shi, X.-Y., Zhang, C.-S., Wang, L.-S., Huang, S., Liu, D.-S., 2011. [Temporal and spatial distribution of particulate organic carbon in the Yellow Sea and East China Sea in spring]. Huan jing ke xue= Huanjing kexue 32, 2505–11.

Cloern, J.E., 1996. Phytoplankton bloom dynamics in coastal ecosystems: a review with some general lessons from sustained investigation of San Francisco Bay, California. Rev. Geophys. 34, 127–168.

Cong, P., Qu, L., Han, G., Yang, X., 2012. Remotely sensed detection and application analysis of ocean particulate organic carbon. Mar. Environ. Sci. 31, 300–304.

Dalsgaard, T., 2003. Benthic primary production and nutrient cycling in sediments with benthic microalgae and transient accumulation of macroalgae. Limnol. Oceanogr. 48, 2138–2150.

De Jonge, V.N., Colijn, F., 1994. Dynamics of microphytobenthos biomass in the Ems estuary. Mar. Ecol. Prog. Ser. 185–196.

Den Hartog, C., 1970. The sea-grasses of the world. North-Holland, Amsterdam.

Duan, H., Feng, L., Ma, R., Zhang, Y., Arthur Loiselle, S., 2014. Variability of particulate organic carbon in inland waters observed from MODIS Aqua imagery. Environ. Res. Lett. 9. https://doi.org/10.1088/1748-9326/9/8/084011

Evers-King, H., Martinez-Vicente, V., Brewin, R.J.W., Dall'Olmo, G., Hickman, A.E., Jackson, T., Kostadinov, T.S., Krasemann, H., Loisel, H., Röttgers, R., Roy, S., Stramski, D., Thomalla, S., Platt, T., Sathyendranath, S., 2017. Validation and intercomparison of ocean color algorithms for estimating particulate organic carbon in the oceans. Front. Mar. Sci. 4, 1–20. https://doi.org/10.3389/fmars.2017.00251

Fan, H., Wang, X., Zhang, H., Yu, Z., 2018. Spatial and temporal variations of particulate organic carbon in the Yellow-Bohai Sea over 2002-2016. Sci. Rep. https://doi.org/10.1038/s41598-018-26373-w

Fernandes, L., Bhosle, N.B., Matondkar, S.G.P., Bhushan, R., 2009. Seasonal and spatial distribution of particulate organic matter in the Bay of Bengal. J. Mar. Syst. 77, 137–147.

Fingas, M., 2018. Remote Sensing for Marine Management, in: World Seas: An Environmental Evaluation. Elsevier, pp. 103–119. https://doi.org/10.1016/b978-0-12-805052-1.00005-x

Fonseca, M.S., Kenworthy, W.J., 1987. Effects of current on photosynthesis and distribution of seagrasses. Aquat. Bot. 27, 59–78.

Gaiser, P.W., Member, S., Germain, K.M.S., Member, S., Twarog, E.M., Poe, G.A., Purdy, W., Richardson, D., Grossman, W., Jones, W.L., Spencer, D., Golba, G., Cleveland, J., Choy, L., Bevilacqua, R.M., Chang, P.S., Member, S., 2004. The WindSat Spaceborne Polarimetric Microwave Radiometer : Sensor Description and Early Orbit Performance. IEEE Trans. Geosci. Remote Sens. 42.

Gardner, W.D., Mishonov, A. V., Richardson, M.J., 2006. Global POC concentrations from in-situ and satellite data. Deep. Res. Part II Top. Stud. Oceanogr. 53, 718–740. https://doi.org/10.1016/j.dsr2.2006.01.029

Gomes, H.R., Goes, J.I., Saino, T., 2000. Influence of physical processes and freshwater discharge on the seasonality of phytoplankton regime in the Bay of Bengal. Cont. Shelf Res. 20, 313–330. https://doi.org/10.1016/S0278-4343(99)00072-2

Gould, D.M., Gallagher, E.D., 1990. Field measurement of specific growth rate, biomass, and primary production of benthic diatoms of Savin Hill Cove, Boston. Limnol. Oceanogr. 35, 1757–1770.

Green, E.P., Short, F.T., Frederick, T., 2003. World atlas of seagrasses. Univ of California Press.

Haibo, Z., Luning, Y., Lisha, W., Shaofeng, P., Xiaoyong, S., 2016. Distribution and source analyses of particulate organic carbon in the Yellow Sea and Bohai Sea during summer, 2013. Haiyang Xuebao 38, 24–35.

He, X., Bai, Y., Pan, D., Huang, N., Dong, X., Chen, J., Chen, C.T.A., Cui, Q., 2013. Using geostationary satellite ocean color data to map the diurnal dynamics of suspended particulate matter in coastal waters. Remote Sens. Environ. 133, 225–239. https://doi.org/10.1016/j.rse.2013.01.023

Hemminga, M.A., Duarte, C.M., 2000. Seagrass ecology. Cambridge University Press.

Hussain, M.G., Failler, P., Al Karim, A., Alam, M.K., 2017. Review on opportunities, constraints and challenges of blue economy development in Bangladesh. J. Fish. Life Sci. 2, 45–57.

Jeremy Werdell, P., McClain, C.R., 2019. Satellite remote sensing: Ocean color, 3rd ed, Encyclopedia of Ocean Sciences. Elsevier Inc. https://doi.org/10.1016/B978-0-12-409548-9.10817-6

Kavak, M.T., Karadogan, S., 2011. The relationship between sea surface temperature and chlorophyll concentration of phytoplanktons in the Black Sea using remote sensing techniques Author Details. J. Environ. Biol 32, 493–498.

Khatun, M.A., Rashid, M.B., Hygen, H.O., 2016. Climate of Bangladesh. MET Rep. 2387–4201.

Knap, A.H., Michaels, A., Close, A.R., Ducklow, H., Dickson, A.G., 1996. Protocols for the joint global ocean flux study (JGOFS) core measurements.

Le, C., Lehrter, J.C., Hu, C., MacIntyre, H., Beck, M.W., 2017. Satellite observation of particulate organic carbon dynamics in two river-dominated estuaries. J. Geophys. Res. Ocean. 122, 555–569. https://doi.org/10.1002/2016JC012275

Le, C., Zhou, X., Hu, C., Lee, Z., Li, L., Stramski, D., 2018. A Color-Index-Based Empirical Algorithm for Determining Particulate Organic Carbon Concentration in the Ocean From Satellite Observations. J. Geophys. Res. Ocean. 123, 7407–7419. https://doi.org/10.1029/2018JC014014

Lee, D., Jeong, J.-Y., Jang, H.K., Min, J.-O., Kim, M.J., Youn, S.H., Lee, T., Lee, S.H., 2019. Comparison of Particulate Organic Carbon to Chlorophyll-a Ratio Based on the Ocean Color Satellite Data at the Ieodo and Socheongcho Ocean Research Stations. J. Coast. Res. 90, 267. https://doi.org/10.2112/si90-033.1

Liu, D., Bai, Y., He, X., Pan, D., Chen, C.T.A., Li, T., Xu, Y., Gong, C., Zhang, L., 2019a. Satellite-derived particulate organic carbon flux in the Changjiang River through different stages of the Three Gorges Dam. Remote Sens. Environ. 223, 154–165. https://doi.org/10.1016/j.rse.2019.01.012

Liu, D., Bai, Y., He, X., Tao, B., Pan, D., Chen, C.T.A., Zhang, L., Xu, Y., Gong, C., 2019b. Satellite estimation of particulate organic carbon flux from Changjiang River to the estuary. Remote Sens. Environ. 223, 307–319. https://doi.org/10.1016/j.rse.2019.01.025

Liu, D., Pan, D., Bai, Y., He, X., Wang, D., Wei, J.A., Zhang, L., 2015. Remote sensing observation of particulate organic carbon in the Pearl River Estuary. Remote Sens. 7, 8683–8704. https://doi.org/10.3390/rs70708683

Lucas, L. V, Cloern, J.E., 2002. Effects of tidal shallowing and deepening on phytoplankton production dynamics: A modeling study. Estuaries 25, 497–507.

Madhu, N. V, Maheswaran, P.A., Jyothibabu, R., Sunil, V., Revichandran, C., Balasubramanian, T., Gopalakrishnan, T.C., Nair, K.K.C., 2002. Enhanced biological production off Chennai triggered by October 1999 super cyclone (Orissa), CURRENT SCIENCE. Indian Academy of Sciences.

Malone, T.C., Crocker, L.H., Pike, S.E., Wendler, B.W., 1988. Influences of river flow on the dynamics of phytoplankton production in a partially stratified estuary. Mar. Ecol. Prog. Ser. Oldend. 48, 235–249.

Marra, J.F., Dickey, T.D., Plueddemann, A.J., Weller, R.A., Kinkade, C.S., Stramska, M., Phytoplankton, M., 2015. Phytoplankton bloom phenomena in the North Atlantic Ocean and Arabian Sea. North Atl. Ocean Arab. Sea.-ICES J. Mar. Sci. 72, 2021–2028.

https://doi.org/10.1093/icesjms/fsu241

Menzel, D.W., 1974. Primary productivity, dissolved and particulate organic matter, and the sites of oxidation of organic matter. Sea. Mar. Chem. 5, 654–678.

Murray, J.W., 2000. The oceans, International Geophysics. https://doi.org/10.1016/S0074-6142(00)80116-3

Nagamani, P. V., Shikhakolli, R., Chauhan, P., 2011. Phytoplankton Variability in the Bay of Bengal During Winter Monsoon Using Oceansat-1 Ocean Colour Monitor Data. J. Indian Soc. Remote Sens. 39, 117–126. https://doi.org/10.1007/s12524-010-0056-0

Nandakumar, K., Venkat, K., Bhosle, N.B., 1987. Distribution of particulate organic carbon in the central Bay of Bengal. Proc. Indian Acad. Sci. - Earth Planet. Sci. 96, 189–193. https://doi.org/10.1007/BF02839268

NASA, 2014a. Chlorophyll a (chlor_a) [WWW Document]. NASA. URL https://oceancolor.gsfc.nasa.gov/atbd/chlor_a/ (accessed 2.21.20).

NASA, 2014b. Long-Wave Sea Surface Temperature (SST) [WWW Document]. NASA. URL https://oceancolor.gsfc.nasa.gov/atbd/sst/ (accessed 2.21.20).

Nowlin, W.D., Jochens, A.E., DiMarco, S.F., Reid, R.O., Howard, M.K., 2005. Low-frequency circulation over the Texas-Louisiana continental shelf. Geophys. Monogr. Geophys. UNION 161, 219.

O'Donohue, M.J.H., Dennison, W.C., 1997. Phytoplankton productivity response to nutrient concentrations, light availability and temperature along an Australian estuarine gradient. Estuaries 20, 521–533.

Parsons, T.R., Maita, Y., Lalli, C.M., 1984. A manual of chemical and biological methods for seawater analysis. Pergamon Press.

Pavia, F.J., Anderson, R.F., Lam, P.J., Cael, B.B., Vivancos, S.M., Fleisher, M.Q., Lu, Y., Zhang, P., Cheng, H., Lawrence Edwards, R., 2019. Shallow particulate organic carbon regeneration in the South Pacific Ocean. Proc. Natl. Acad. Sci. U. S. A. 116, 9753–9758. https://doi.org/10.1073/pnas.1901863116

Pinckney, J.L., Zingmark, R.G., 1993. MODELING THE ANNUAL PRODUCTION OF

INTERTIDAL BENTHIC MICROALGAE IN ESTUARINE ECOSYSTEMS 1. J. Phycol. 29, 396–407.

Rizzo, W.M., Lackey, G.J., Christian, R.R., 1992. Significance of euphotic, subtidal sediments to oxygen and nutrient cycling in a temperate estuary. Mar. Ecol. Prog. Ser. Oldend. 86, 51–61.

Roca, M., Chen, K., Pérez-Gálvez, A., 2016. Chlorophylls, in: Handbook on Natural Pigments in Food and Beverages: Industrial Applications for Improving Food Color. Elsevier Inc., pp. 125–158. https://doi.org/10.1016/B978-0-08-100371-8.00006-3

Sarangi, R.K., Devi, K.N., 2017. Space-based observation of chlorophyll, sea surface temperature, nitrate, and sea surface height anomaly over the Bay of Bengal and Arabian Sea. Adv. Sp. Res. 59, 33–44. https://doi.org/10.1016/j.asr.2016.08.038

Sarangi, R.K., Nayak, S., Panigrahy, & R.C., 2008. Monthly variability of chlorophyll and associated physical parameters in the southwest Bay of Bengal water using remote sensing data, Indian Journal of Marine Sciences.

Sharp, J.H., 1974. Improved analysis for "particulate" organic carbon and nitrogen from seawater1. Limnol. Oceanogr. 19, 984–989. https://doi.org/10.4319/lo.1974.19.6.0984

Shen, Zhiliang; Yang, Heming & Liu, Q., 2020. Particulate Organic Carbon and Its Composition in Jiaozhou Bay. Springer Berlin Heidelberg. https://doi.org/10.1007/978-3-662-58169-8_18

Shen, F., Zhou, Y., Li, J., He, Q., Verhoef, W., 2013. Remotely sensed variability of the suspended sediment concentration and its response to decreased river discharge in the Yangtze estuary and adjacent coast. Cont. Shelf Res. https://doi.org/10.1016/j.csr.2013.09.002

Shi, X., Zhang, T., Zhang, C., Cheng, J., 2011. Spatial and temporal distribution of particulate organic carbon in Yellow Sea and East China Sea. Mar. Environ. Sci. 1.

Siegel, D.A., Behrenfeld, M.J., Maritorena, S., McClain, C.R., Antoine, D., Bailey, S.W., Bontempi, P.S., Boss, E.S., Dierssen, H.M., Doney, S.C., Eplee, R.E., Evans, R.H., Feldman, G.C., Fields, E., Franz, B.A., Kuring, N.A., Mengelt, C., Nelson, N.B., Patt, F.S., Robinson, W.D., Sarmiento, J.L., Swan, C.M., Werdell, P.J., Westberry, T.K.,

Wilding, J.G., Yoder, J.A., 2013. Regional to global assessments of phytoplankton dynamics from the SeaWiFS mission. Remote Sens. Environ. 135, 77–91. https://doi.org/10.1016/j.rse.2013.03.025

Stramska, M., 2014. Particulate organic carbon in the surface waters of the North Atlantic: Spatial and temporal variability based on satellite ocean colour. Int. J. Remote Sens. 35, 4717–4738. https://doi.org/10.1080/01431161.2014.919686

Stramska, M., 2009. Particulate organic carbon in the global ocean derived from SeaWiFS ocean color. Deep. Res. Part I Oceanogr. Res. Pap. 56, 1459–1470. https://doi.org/10.1016/j.dsr.2009.04.009

Stramska, M., Bialogrodzka, J., 2016. Satellite observations of seasonal and regional variability of particulate organic carbon concentration in the Barents Sea. Oceanologia 58, 249–263. https://doi.org/10.1016/j.oceano.2016.04.004

Stramski, D., Reynolds, R.A., Babin, M., Kaczmarek, S., Lewis, M.R., Röttgers, R., Sciandra, A., Stramska, M., Twardowski, M.S., Franz, B.A., Claustre, H., 2008. Relationships between the surface concentration of particulate organic carbon and optical properties in the eastern South Pacific and eastern Atlantic Oceans, Biogeosciences.

Stramski, D., Reynolds, R.A., Kahru, M., Mitchell, B.G., 1999a. Estimation of particulate organic carbon in the ocean from satellite remote sensing. Science (80-.). 285, 239–242. https://doi.org/10.1126/science.285.5425.239

Stramski, D., Reynolds, R.A., Kahru, M., Mitchell, B.G., 1999b. Estimation of particulate organic carbon in the ocean from satellite remote sensing. Science (80-.). 285, 239–242.

Sullivan, M.J., Moncreiff, C.A., 1990. Edaphic algae are an important component of salt marsh food-webs: evidence from multiple stable isotope analyses. Mar. Ecol. Prog. Ser. Oldend. 62, 149–159.

Świrgoń, M., Stramska, M., 2015. Comparison of in situ and satellite ocean color determinations of particulate organic carbon concentration in the global ocean. Oceanologia 57, 25–31. https://doi.org/10.1016/j.oceano.2014.09.002

Tang, D., Satyanarayana, B., Singh, R.P., Zhao, H., 2010. Satellite Remote Sensing of

chlorophyll-a distribution in the Northeast Arabian Sea.

Thompson, P.A., 1998. Spatial and temporal patterns of factors influencing phytoplankton in a salt wedge estuary, the Swan River, Western Australia. Estuaries 21, 801–817.

Walton, C.C., Pichel, W.G., Sapper, J.F., May, D.A., 1998. The development and operational application of nonlinear algorithms for the measurement of sea surface temperatures with the NOAA polar-orbiting environmental satellites. J. Geophys. Res. Ocean. 103, 27999–28012. https://doi.org/10.1029/98JC02370

Wang, X., Ma, H., Li, R., Song, Z., Wu, J., 2012. Seasonal fluxes and source variation of organic carbon transported by two major Chinese Rivers: The Yellow River and Changjiang (Yangtze) River. Global Biogeochem. Cycles 26. https://doi.org/10.1029/2011GB004130

Wangersky, P.J., 1977. The role of particulate matter in the productivity of surface waters. Helgoländer Wissenschaftliche Meeresuntersuchungen 30, 546–564. https://doi.org/10.1007/BF02207860

Ward, L.G., Kemp, W.M., Boynton, W.R., 1984. The influence of waves and seagrass communities on suspended particulates in an estuarine embayment. Mar. Geol. 59, 85–103.

Webster, I.T., Ford, P.W., Hodgson, B., 2002. Microphytobenthos contribution to nutrient-phytoplankton dynamics in a shallow coastal lagoon. Estuaries 25, 540–551.

Wentz, F.J., L.Ricciardulli, C.Gentemann, T. Meissner, K.A. Hilburn, J.S., 2013. Remote Sensing Systems Coriolis WindSat [indicate whether you used Daily, 3-Day, Weekly, or Monthly] Environmental Suite on 0.25 deg grid, Version 7.0.1, [indicate subset if used]. Remote Sensing Systems, Santa Rosa, CA [WWW Document]. URL http://www.remss.com/missions/windsat/ (accessed 3.22.20).

Wetzel, R.G., 1995. Death, detritus, and energy flow in aquatic ecosystems. Freshw. Biol. 33, 83–89. https://doi.org/10.1111/j.1365-2427.1995.tb00388.x

Williams, P.J.L.E., 1975. Biological and chemical aspects of dissolved oraganic materials in seawater. Chem. Oceanogr. 301–363.

Williams, P.M., 1971. The distribution and cycling of organic matter in the ocean. In,

Organic Compounds in Aquatic Environment. SJ FAUST and JV HUNTER (eds.) 145-163.

Xie, F., Tao, Z., Zhou, X., Lv, T., Wang, J., 2019. Spatial and Temporal Variations of Particulate Organic Carbon Sinking Flux in Global Ocean from 2003 to 2018. Remote Sens. 11, 2941. https://doi.org/10.3390/rs11242941

Xu, K., Milliman, J.D., 2009. Seasonal variations of sediment discharge from the Yangtze River before and after impoundment of the Three Gorges Dam. Geomorphology 104, 276–283. https://doi.org/10.1016/j.geomorph.2008.09.004

Yoder, J., Kennelly, M., 2006. What Have We Learned About Ocean Variability from Satellite Ocean Color Imagers? Oceanography 19, 152–171. https://doi.org/10.5670/oceanog.2006.98

Yu, J., Wang, X., Fan, H., Zhang, R.H., 2019. Impacts of Physical and Biological Processes on Spatial and Temporal Variability of Particulate Organic Carbon in the North Pacific Ocean during 2003–2017. Sci. Rep. 9, 1–15. https://doi.org/10.1038/s41598-019-53025-4

Zhu, G.H., Liu, Y.L., Chen, L.H., Yu, P.S., Jin, M., Liu, Z.L., 2011. Studies on Phytoplankton and Particulate Organic Carbon in the Southern Ocean. Appl. Mech. Mater. 137, 344–352. https://doi.org/10.4028/www.scientific.net/amm.137.344

Zibordi, G., Mélin, F., 2017. An evaluation of marine regions relevant for ocean color system vicarious calibration. Remote Sens. Environ. 190, 122–136. https://doi.org/10.1016/j.rse.2016.11.020

8. Annex

Section I

Special apparatus and equipment and regents:

- Spectrophotometer
- 1-cm path length quartz cuvettes
- 0.45 µm pore size nitrocellulose filter with a 47-mm diameter
- Aluminum foil
- 50-ml stoppered graduated cylinders
- 30-ml Pyrex beakers with cover glasses
- Hot plate & magnetic stirrer at 100 °C
- GPS tracker
- Sampler
- A vacuum pump or source capable of maintaining a vacuum up to 6 in. Hg
- Freezer capable of freeze in -20°C
- Sulfuric acid-dichromate oxidant
- Analytical reagent grade (70%) phosphoric acid
- Sodium sulfate solution &
- Distilled water

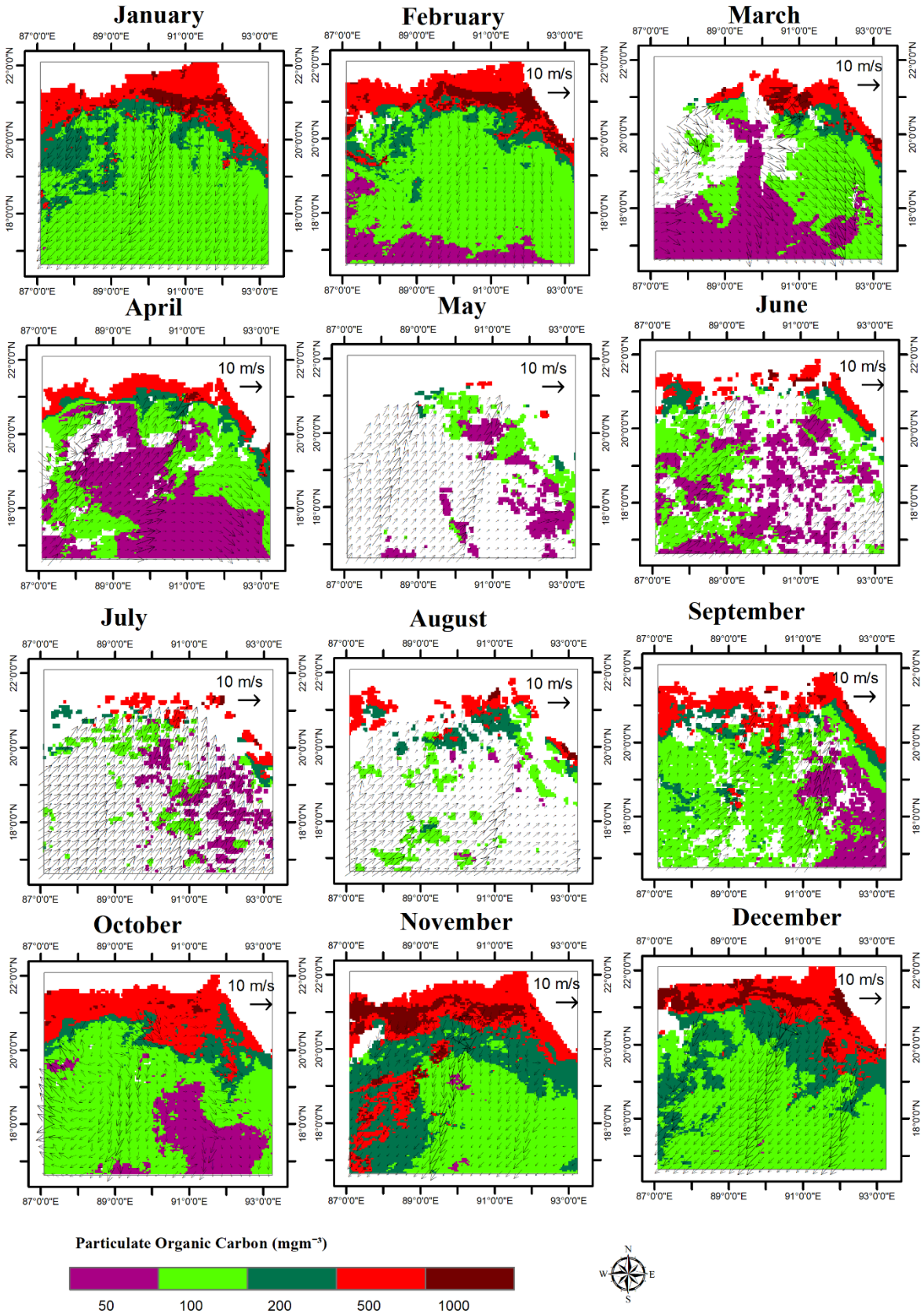

Fig. 15 WindSat derived monthly relationship between POC and wind vector in 2019

Fig. 16 Cruise vessel (BNS Turag)

Fig. 17 Setting filter paper with the suction tube

Fig. 18 Spectrophotometric measurement of sample